

Simultaneous Hydrogen Formation and Pollutant Degradation over Pt-modified Morphology Controlled ZnSe Photocatalyst



By

Ayesha Nudrat

NUST201463667MSNS78214F

**This work is submitted as an MS thesis in partial fulfillment of the
requirement for the degree of**

MS in Chemistry

Supervised By: Dr. Muhammad Fahad Ehsan

Co-supervisor: Dr. Muhammad Arfan

Department of Chemistry

School of Natural Sciences (SNS)

National University of Sciences and Technology H-12,

Islamabad, Pakistan

2017

National University of Sciences & Technology

MS THESIS WORK

We hereby recommend that the dissertation prepared under our supervision by: AYESHA NUDRAT, Regn No. NUST201463667MSNS78214F Titled: Simultaneous Hydrogen Formation and Pollutant Degradation over Pt-modified Morphology Controlled ZnSe Photocatalyst be accepted in partial fulfillment of the requirements for the award of **MS** degree.

Examination Committee Members

1. Name: Dr. Syed Rizwan Hussain

Signature: 

2. Name: Dr. Iftikhar H. Gul

Signature: 


External Examiner: Dr. Saira Arif

Signature: 

Co-Supervisor: Dr. Muhammad Arfan

Signature: 

Supervisor's Name: Dr. M. Fahad Ehsan

Signature: 


Head of Department

24-11-17
Date

COUNTERSIGNED

Date: 24/11/17


Dean/Principal

THESIS ACCEPTANCE CERTIFICATE

Certified that final copy of MS thesis written by Ms. Ayesha Nudrat, (Registration No. NUST201463667MSNS78214F), of School of Natural Sciences has been vetted by undersigned, found complete in all respects as per NUST statutes/regulations, is free of plagiarism, errors, and mistakes and is accepted as partial fulfillment for award of MS/M.Phil degree. It is further certified that necessary amendments as pointed out by GEC members and external examiner of the scholar have also been incorporated in the said thesis.

Signature: _____ 

Name of Supervisor: Dr. M. Fahad Ehsan

Date: _____

Signature (HoD): _____ 

Date: 24-11-17

Signature (Dean/Principal): _____ 

Date: 24/11/17

Dedicated to

My Beloved Parents and Siblings

Acknowledgements

First and foremost, I would say thanks to **The All-powerful Allah** to give me the understanding, capacity and opportunity to undertake and continue this research study as well as to complete it satisfactorily. Without His favors, this achievement would certainly not have been possible. There are so many people to thank in so many ways.

I am particularly indebted to my adviser, **Dr. Muhammad Fahad Ehsan**, for his continuous support, patience and optimism to make it possible to compose this thesis. He not just put colossal amount of time and efforts into directing this research but also coordinated in altering and confirming every aspect of research results to most modest level of detail.

I would also extend my gratitude to all GEC members including **Dr. Muhammad Arfan, Dr. Rizwan Hussain, Dr. Iftikhar Hussain Gul** for their constructive criticism and suggestions for the improvement of thesis. I greatly acknowledge the facilities and technical support provided by the SNS, Principal SNS **Prof. Azad Siddiqui** and HoD Chemistry Department **Prof. Habib Nasir**. I am also thankful to the Chemistry Lab staff for their technical support.

And finally, I would like to express gratitude to my parents, my siblings, my teachers and my dear friends.

Ayesha Nudrat

Abbreviations and Symbols

ZnSe	Zinc Selenide
Pt	Platinum
TiO ₂	Titanium Dioxide
KOH	Potassium Hydroxide
H ₂	Molecular Hydrogen
Na ₂ S	Sodium Sulphide
CH ₃ OH	Methanol
SEM	Scanning Electron Microscopy
EDS	Energy Dispersive Spectrometry
XRD	X-ray Powder Diffraction
TEM	Transmission Electron Microscopy
UV-Vis	Ultra Violet -Visible
PL	Photoluminescence
nm	Nanometer
PV	Photovoltaic
Å	Angstrom

Abstract

In this tentative work, various ZnSe photocatalysts were synthesized employing hydrothermal route. Different parameters like reaction temperature, reaction time and concentration of KOH were optimized to observe the effect of these factors on morphology of photocatalysts. The optical and morphological properties of as synthesized nanostructures were studied using X-ray Diffraction Spectroscopy (XRD), Scanning Electron Microscopy (SEM), UV-Vis spectroscopy, Transmission Electron Microscopy (TEM) and Energy Dispersive X-ray Spectroscopy (EDS) for elemental analysis. Spherical morphology for ZnSe nanoparticles was seen in SEM studies, the size of particle was affected significantly by change in reaction temperature and KOH conc. Whereas, change in reaction time showed no significant effect on morphology or size of nanoparticles. Average particle size was around 28 nm confirmed by SEM and TEM analysis. This ZnSe photocatalyst was then investigated simultaneously for H₂ formation and for degradation of organic pollutants such as CH₃OH and Na₂S under illumination of different lights. Low hydrogen production (3 μmol/h) was observed in case of bare ZnSe. In order to enhance the photocatalyst efficiency and to reduce the e⁻/h⁺ recombination, 1% by wt. Pt was introduced via in situ photoreduction due. This metallized ZnSe/Pt photocatalyst was exposed to Na₂S and CH₃OH solutions under UV and visible light. A maximum of hydrogen formation rate of about 30 μmol/h and 17 μmol/h was observed in case of methanol and sodium sulphide, respectively.

Contents

Chapter 1	1
Introduction and Literature Review	1
1.1 Energy in Today's World.....	1
1.1.1 Fossil Fuels.....	2
1.1.2 Hydrothermal Energy.....	2
1.1.3 Wind Energy	3
1.1.4 Nuclear Energy.....	3
1.1.5 Geothermal Energy	3
1.1.6 Solar Energy.....	4
1.2 Harvesting Solar Energy.....	5
1.2.1 Solar/Photovoltaic Cells.....	5
1.2.2 Solar Thermal.....	6
1.2.3 Natural Photosynthesis.....	6
1.2.4 Artificial Photosynthesis	6
1.3 Hydrogen Evolution by Solar Energy.....	8
1.4 Solar Water Splitting.....	9
1.5 Photocatalysis	6
1.6 Photo catalysts for Hydrogen production by Water Splitting.....	9
1.7 Application of Solar Energy for Removal of Hazardous Chemicals In Water.....	11
1.7.1 Photocatalytic Degradation of Organic Dyes.....	12
1.8 Simultaneous Production of Molecular Hydrogen (H ₂) And Degradation of Dyes	16
1.9 Factors that Effect Photocatalytic Efficiency	18

1.9.1 Co-catalyst Addition to Photocatalysts	19
1.10 ZnSe As a Semiconductor Photocatalyst	20
1.10.1 Potential Applications of ZnSe	20
1.10.1.1 LEDs	20
1.10.1.2 Lasers	22
1.10.1.3 Photodetectors	22
1.10.1.4 Field Emitters	23
1.10.1.5 Sensors	23
1.10.1.6 Photocatalysis	24
1.10.1.7 Doped Semiconductors	26
1.10.1.8 Vivo Imaging	26
Chapter 2	28
Experimental and Characterization Techniques	28
2.1 Chemicals	28
2.2 Synthesis of Nanoparticles	28
2.2.1 Gas Condensation	29
2.2.2 Vacuum Deposition and Vaporization	30
2.2.3 Chemical Vapor Deposition (CVD) and Chemical Vapor Condensation (CVC)	30
2.2.4. Mechanical Attrition	30
2.2.5 Chemical Precipitation	31
2.2.6 Sol-Gel Techniques	31
2.2.7 Electrodeposition	32
2.2.8 Hydrothermal Process	32

2.3 Sample Preparation	32
2.4 ZnSe modification with Pt and Photoactivity Tests	34
2.5 Characterization Techniques	34
2.5.1 X-ray Diffraction Crystallography	35
2.5.2 Scanning Electron Microscope	36
2.5.3 UV-Vis Absorbance Spectroscopy	36
2.5.4 Transmission Electron Microscopy (TEM)	37
2.5.5 Energy Dispersive X-ray Spectrometry.....	37
Chapter 3	38
Results and Discussion	38
3.1 Effect of Reaction Conditions on ZnSe.....	38
3.1.1 Effect of Temperature.....	38
3.1.2. Effect of KOH Concentration.....	40
3.1.3. Effect of Reaction Time	42
3.2 Phase and Morphological Results for ZnSe,ZnSe/Pt	44
3.3 Optical Analysis	45
3.4 Transmission Electron Microscopy (TEM) Results.....	46
3.5 Compositional Analysis	47
3.6 Photocatalytic Activity	48
Chapter 4	59
4.1 Conclusions and Future Prospects.....	59
References	54

List of Tables

Table 2.1 List of Chemicals for Synthesis of ZnSe Nanoparticles.....	27
Table 2.2 ZnSe Synthesized by Changing Reaction Temperatures.....	32

List of Figures

Figure 1.1 Schematic Illustration of a Photocatalytic Reaction.....	7
Figure 1.2 Water Splitting Photo activity of ZnGeO ₄ Loaded with Co-catalysts Pt and RuO ₂ Respectively.....	20
Figure 1.3 fuchsine acid solution (color changes and absorption spectra) in the presence of ZnSe nanobelts under exposure to UV light: a) initially prepared solution; b–h) solutions after adding ZnSe nanobelts	24
Figure 3.1 XRD Patterns of ZnSe Samples Obtained at (a) 120°C, (b) 140°C, (c) 160°C, (d) 180°C, (e) 200°C.....	39
Figure 3.2 SEM Images of As-synthesized ZnSe Microspheres at (a) 120 °C, (b) 140 °C, (c) 160 °C, (d) 180 °C and (e) 200 °C.....	40
Figure 3.3 XRD Patterns for As-synthesized ZnSe Nanoparticles at KOH Conc. of (a)2M,(b)3M,(c)4M,(d)5M,(e)6M.....	41
Figure 3.4 SEM Images for ZnSe Microspheres Synthesized using KOH (a) 2M, (b) 3M, (c) 4M (d) 5M, (e) 6M.....	42
Figure 3.5 XRD Patterns of ZnSe Nanoparticles Synthesized at Reaction Temperatures (a)1 hr, (b)3h, (c)5h, (d)7h, (e) 9h.....	43
Figure 3.6 SEM Images for ZnSe Obtained at Reaction Time (a) 1h, (b) 3h, (c) 5h, (d) 7h,(e)9h.....	44
Figure 3.7 XRD and SEM Patterns of ZnSe Photocatalysts using 6M KOH Solution and Hydrazine Hydrate at 200 °C for 3 h.....	45
Figure 3.8 UV-Visible Spectra, Tauc Plot and Band Alignment for ZnSe Prepared using 6M KOH at 200°C for 3 h.....	46
Figure 3.9 TEM Image for as Synthesized ZnSe Nanostructures.....	47
Figure 3.10 EDS Spectra of ZnSe Nanoparticles.....	48

Figure 3.11 Hydrogen Formation Rate as a Function of Time of Irradiation (a) When Bare ZnSe Photocatalyst was Exposed to Methanol under Illumination of UV Light.....50

Figure 3.12 Band Alignment Diagram ZnSe, ZnSe/Pt Photocatalyst.....51

Figure 3.13 (b) When Pt/ZnSe Exposed to Methanol Solution under Illumination of UV Light (c) Pt/ZnSe Exposed to Methanol Solution under Illumination of UV/Visible Sunlight (d) ZnSe/Pt Exposed to Sodium Sulphide Solution under Illumination of Visible Light.....52

Chapter 1

Introduction and Literature Review

1.1 Energy in Today's World

Energy is an unpreventable part of today's society and economy. Achievement of each work relies on the adequate and unremitting supply of energy. With the advent of low-cost automobile and the spread of electricity, world's energy needs have changed drastically. Energy use is growing quickly each year with a sharp decline in cost of energy. So far, fossil fuels provide a valuable service in coping up with these energy needs. The problem does not lie with the usage of fossil fuels but with consequences of using them in form of pollution and depletion of non-renewable resources. It is estimated that on an average earth's temperature is rising 1°F. On the other hand, this era has seen most productive population and industrial development and improvement in terms of economics — which was and still remains absolutely subject to the utilization of energy. In 2013, it was estimated that world's energy utilization was about 17 TW and is estimated to be doubled by 2050 [1].

Advancement of an efficient and renewable energy supply is critical to alleviate outcomes of fossil fuel utilization including environmental change, inevitable consumption of fuels and remote oil reliance.[2-4]. There are a few option energy sources such as hydropower, geothermal, wind, nuclear and solar powered which are generally efficient and sustainable in correlation with fossil fuels but all of these have few constraints that make this substitution unreliable. A short comparison of each is energy source is listed below:

1.1.1 Fossil Fuels

There are numerous advantages linked with use of fossil fuels such as:

- Fossil fuels have an ability to generate huge amount of electricity in one place.
- Use of coal is a cost-efficient method for generation of energy as coal is present in abundance.
- Power plants utilizing natural gas are even more efficient and cost effective.
- Power generation plants can be constructed at any place as long as transportation of fuel is possible at that place.

But disadvantages of using fossil fuels outrun their advantages in several ways such as:

- Pollution is the major disadvantage of using fossil fuels. Their consumption results in release of green house gases such as CO₂ thus acting as a contributing factor towards global warming being experienced today.
- Burning of coal results in release of CO₂ and SO₂ which in return cause acid rain
- Mining of coal disrupts the environment and cause destruction in large areas of land.
- Use of crude oil also poses environmental hazards like oil spills in seas due to leakage or drowning of oil tanks

1.1.2 Hydrothermal energy

Water is one of the earth's most abundant resource. It is also used for production of electricity and offers certain advantages such as:

- Use of fossil fuels can be eliminated with use of hydroelectricity, which also gives an advantage that operating cost of plant will not be affected by rise in fossil fuels price.
- Since it does not produce any harmful products as a result of generation of electricity, it does not cause pollution of air and water.
- Hydro-power plants are more durable then fossil fuel plants. Some hydropower plants are being operational for 50 to 100 years.

- Labor cost is also low as the plant is automatic with need for a few people for maintenance of power plant.

On the contrary,

- These power plants tend to affect the surrounding ecosystem, dams, for example have found to reduce the fish population.
- High construction cost of dams is also a concern. Not to mention the number of political and regional conflicts associated with building dams.
- Another problem is the emission of CH₄ and CO₂ in power plant reservoirs located in tropical areas.

1.1.3 Wind Energy

- Wind energy is beneficial because it is a clean source of energy production and does not cause any air or land pollution.
- But it has limitations in terms of not being able to store generated electricity and adverse effect on population of wild birds.

1.1.4 Nuclear Energy

- Generation of electricity through nuclear power is relatively cleaner than burning of fossil fuels, except for the small amount of radioactive emissions caused by processing of Uranium.
- Its main problem that concerns the environment is its by-product wastes which are greatly radio-active. This also includes the tools and instruments which have been contaminated by radioactivity during processing.

1.1.5 Geothermal Energy

- When compared with other energy sources, geothermal energy offers a relatively cleaner and environment friendly solution. As this is a natural resource therefore it is

available in abundance and have lesser emissions of harmful chemicals into the environment.

- Economically speaking, this is a cost effective method as its price is not affected by fluctuations in fuel prices.

On the contrary, it has certain disadvantages such as:

- Geothermal fluids can cause corrosion and operates at low temperatures, which in turn can limit the efficiency of heat engines for electricity production.
- The stability of neighboring land is greatly affected where the geothermal power station is installed.
- And lastly, the stations which have provided energy for a long period of time may eventually cool down possibly because the power station was so large that it utilized all of the earth's thermal energy.

1.1.6 Solar Energy

The only reliable source which is also unlimited and free is solar energy. It offers production of heat and electricity without any maintenance and storage issues. The energy consumption of one year could be generated by solar irradiation of thirty minutes on earth [5], it offers advantages in a number of ways:

- Solar energy is free of cost and it does not involve any environmental pollution. It does not produce any harmful byproducts and is available as long as the sun shines.
- Solar systems can work under any climate and at any location although orientation needs to be considered.
- It is also not dependent on supply of fuels; therefore, cost price is not affected by any increase or decrease in fuel costs.
- Sun is cost free source of energy with no noise pollution while generating power. And transportation of solar energy to the earth does not require any wires therefore solar

power plants can be installed in remote areas easily without any need for central grid stations.

- Solar panels are durable and require less maintenance which results in saving of resources. Originally invested amount can be recovered in a shorter time as energy cost becomes zero.

However,

- Amount of solar radiations reaching the earth is dependent on geographical location, time day and season [6,7].
- The initial investment price for installation of solar energy planet is quite high.
- Another disadvantage includes low solar energy density per unit of Earth surface [8]. Therefore, it is crucial to develop a method so that solar energy can be harvested efficiently.

1.2 Solar Energy Harvesting

The sun is the source of infinite renewable energy. It is the largest source of renewable energy present in our environment. Therefore, vast research has been done in order to maximize its harvesting, storage and utilization solar energy. The solar energy can be harvested in one of the following four ways

1.2.1 Solar/Photovoltaic Cells

Photovoltaic (PV) cells also referred to as solar panels are commonly used for extraction and utilization of solar energy. These cells have been greatly utilized for residential and commercial purposes. PV cells produce energy by exciting electrons in their structures. These cells are mostly semiconductor materials which have an excellent ability to absorb sunlight and generate electric energy. When solar light is absorbed by a semiconductor material, it excites the electrons present in its structure. these electrons can then be utilized in an electric circuit to yield electricity. a basic reason for using semiconductor based solar cells is that it can distribute excited electrons between high and low energy

states. And as the intensity of absorbed solar light increases, number of high energy electrons also increases.

1.2.2 Solar Thermal

Concentrating solar power (CSP) also known as solar thermal is a lesser known method for harvesting solar energy. It is not commonly used for residential and commercial purposes like solar cells are used. However, it offers great potential for application of solar energy on utility purposes. The energy harvesting process in solar thermal is different than solar cells. In CSP, sunlight is concentrated at a single point by directing towards mirrors. This concentrated energy is then utilized for generating steam through boiled water. The generated high energy steam is then used to operate the turbine which in turn generates electricity. Steam powered turbines for electricity generation is an already established technology for generation of electricity at power plants including those operated by use of fossil fuels. The fundamental difference between CSP and other fossil fuels plants is that CSP use renewable energy source for generation of electricity.

1.2.3 Natural Photosynthesis

A major challenge that is being faced in case of PV cells and CSP is their inability to store solar energy effectively and efficiently.

Plants, on the other hand, have the naturally ability of storing sunlight to use in process of photosynthesis. In this process, plants use CO_2 and H_2O to make $\text{C}_6\text{H}_{12}\text{O}_6$ and O_2 in presence of sunlight. These products obtained as a result of photosynthesis are in turn used and refined as chemical fuels and used in different applications such as generation of energy.

1.2.4 Photocatalysis

Many researches have been done to explain the catalyst involved splitting of water into H_2 and O_2 . According to proposed mechanism, reaction initiation takes place when a light photon, with energy equal or greater than the photocatalyst band gap, is absorbed by

semiconductor photocatalyst. It results in origination of electrons and holes with certain potentials. These two reactive species (electron/hole) are then involved in a number of redox reactions on photocatalyst surface [9]. The electronic structure of photocatalyst plays a prominent role in this process. Any semiconductor based photocatalyst consists of a conduction band, and a valence band. Conduction band contains electrons in it which are transferred to valence band after light absorption. The difference between the energies of two bands is termed as band gap energy and represented by E_g . Before the excitation, both electrons and holes are present in valence band. Incidence of light energy greater than band gap energy results in transfer of electrons to conduction band through excitation. This process can be represented in form of an equation as

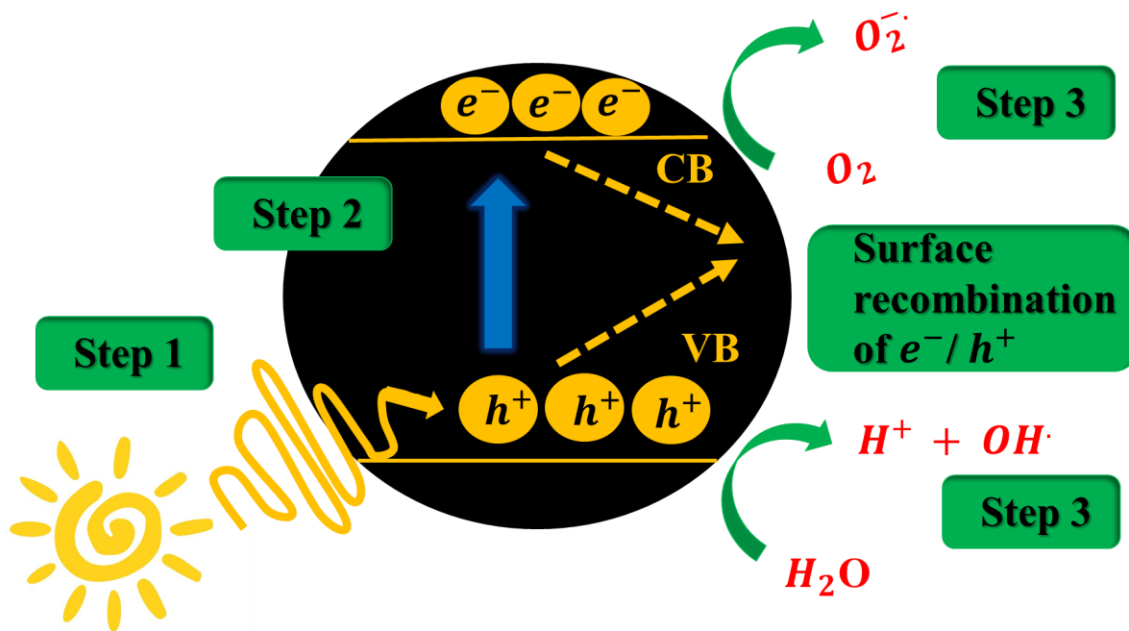
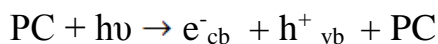


Figure 1.1 Schematic Illustration of a Photocatalytic Reaction

Fujishima A. and Honda K. were the first to report photocatalytic water splitting using titanium dioxide electrode [10]. Since then, a vast number of researches has been carried

out in this field with several different semiconductor photocatalysts being reported. Semiconductor's band gaps lie somewhere in between conductors and insulators. At a point when adequate photochemical energy is provided, electrons (e^-) are energized to conduction band leaving behind holes (h^+) in valence band. These e^-/h^+ pairs play an important role in water splitting redox reactions where electrons assume role of reducing O_2 to O_2^- and holes oxidize water molecules to $OH\cdot$ Radicals both of these species further go on to degrade the organic pollutants.

1.2.5 Artificial Photosynthesis

Artificial photosynthesis uses the same scheme as that of natural photosynthesis and uses a chemical scheme that can convert solar energy into useful chemical fuels. In artificial photosynthesis, natural biological agents are replaced by solid state material that initiate a chemical reaction to produce required fuels.

The only difference between PV cells and solar cells in terms of power generation is that PV cells transport the generated electricity to an external circuit while in solar cells, the produced electricity is used to initiate a chemical reaction at the surface of solid material. The efficiency of chemical reaction can be increased using some catalyst.

1.3 Hydrogen Evolution by Solar Energy

So far, many researchers have tried and generated hydrogen fuel using water splitting by employing the same principle as that of artificial photosynthesis. The hydrogen fuel generated by water splitting can be used in several applications. Hydrogen is an energy source which is not only pure and storable but also renewable and continuous to fulfill global energy demands. Hydrogen has proven very advantageous in several ways like **(1)** it is environment friendly as well as abundant relative to other renewable sources such as water or biomass **(2)** Has high energy yields along with high storage capabilities. Thus an ideal alternate to fossil fuels [11-12],

1.4 Solar water splitting

Solar water splitting is a very suitable process for hydrogen formation. The process uses solar energy and its combination with plentiful water resources [13-15]. There are three ways to split water using sun energy **(1)** photo biological water splitting **(2)** thermochemical water splitting and **(3)** photocatalytic splitting of water. In spite of the fact that the thermochemical approach is the least difficult, the necessity for larger solar powered concentrators make it a technique very costly and less desirable [16]. Bio photolysis can be subcategorized into water bio photolysis and natural bio photolysis depending upon the microorganism type, product, and components of the response [17]. In spite of the fact that water bio photolysis is cleaner than natural bio photolysis (with respect to CO₂ outflows) [18], low hydrogen formation rates, harmful impacts of catalysts, and impediments on scaling up the procedure exist [19]. Water splitting by photocatalysis has a few points of interest over thermochemical and photo biological water part in the way that it is low cost [20], has higher efficiency, capable of isolating H₂ and O₂ streams with relatively smaller reactor size which can easily be used at small scale [21].

1.5 Photocatalysts for Hydrogen Production by Water Splitting

There are several photocatalysts that have been reported and found efficient in water splitting reactions such as TiO₂, ZrO₂, KTaO₃, SrTiO₃ and BiVO₄ as well as SiC, ZnO and CdS along with many others. A brief review of some of these photocatalysts and their hydrogen production efficiency is explained below:

P. Gomathisankar et al. [22] studied the production of hydrogen using TiO₂ as photocatalyst. Different metal particles such as copper, lead, zinc and tin were added to the photo catalyst to check for enhancement in its photoactivity. It was observed that adding copper influenced positively the production rate of Hydrogen. Optimization of reaction temperature, solvent requirements, methanol concentration effect, usage of copper was done. It was estimated that TiO₂/Cu catalyst produced 68 times more hydrogen than that produced by simply using TiO₂ photo catalyst.

A.P.Larios et al. [23] synthesized TiO₂-ZnO photo catalyst employing sol-gel method. The mixed oxide photocatalyst was tested in water splitting for production of Hydrogen. Identification and characterization of prepared sample was done using techniques like nitrogen physisorption, RAMAN, XRD, EDS, XPS and UV-Vis. spectroscopy. Specific surface area studies were performed for all mixed oxides relative to TiO₂. XRD and Raman identified anatase as dominant phase in TiO₂/ZnO. Band gap of synthesized products (3.05-3.12) was in the same range as that of TiO₂ (3.02). photocatalytic activity of synthesized photocatalyst was six times more (1300 μmol/h) than the reference TiO₂ catalyst (190 μmol/h).

Z.Khan and M.Qureshi [24] synthesized Ta doped BaZrO₃ photocatalyst with a cubic phase using precipitation method. Obtained samples BaZr_{1-x}Ta_xO₃ (where x=0, 0.01, 0.02, 0.03, 0.04 and 0.05) were calcinated and characterized by XRD, surface area analysis UV-vis spectroscopy and by photocatalytic activity. Without the addition of any co-catalyst, synthesized photocatalyst BaZr_{1-x}Ta_xO₃ showed efficient hydrogen production under UV-vis light. In a series of experiments, maximum rate of hydrogen production (180 μmol/h) was shown by BaZr_{0.96}Ta_{0.04}O₃ which could be due to greater surface area and reduced band gap.

In the same way, to observe the rate of water splitting, L.M. Martínez et al. [25] synthesized sodium and lanthanum tantalates photocatalyst using sol-gel technique and impregnated with triruthenium dodecarbonyl afterwards. It was observed that impregnation of these tantalates with Ru resulted in an increase in photocatalytic activity by a factor of 25 (4108 H₂ μmol h⁻¹) than that observed in case of La:NaTaO₃ catalyst. Enhanced activity of RuO₂/La:NaTaO₃ catalyst was attributed to the presence of La and RuO₂ in structure of catalyst acting as electron sink for excited electrons generated by UV irradiation. Characterization techniques used were X-ray diffraction for crystal structure (perovskite-type crystalline structure), SEM for particle size (<100nm) and HRTEM for surface structure which showed dispersed RuO₂ particles on tantalate surface.

Yang Liu et al. [26] employed different methods for the synthesis of SrTiO₃ photocatalyst and observed their photo activity under UV light. Surface structure of SrTiO₃ nanoparticles synthesized from all three methods were different. In case of PC method, particle size of SrTiO₃ was small and uniform, solid state method resulted in formation of relatively larger particle size than PC method, while milling assistant method resulted in small sized cubic SrTiO₃ particles. It was also observed that doping of Fe in SrTiO₃ nanoparticles and agglomeration of these nanoparticles only worsened the photo activity of SrTiO₃ particles for Hydrogen evolution. Among the three methods used for synthesis of SrTiO₃ photocatalyst, PC method was best suited for Hydrogen production at an efficient rate (3.2mmolh⁻¹ g⁻¹) as compared to solid state method or milling assisted method. Moreover, cation doped SrTiO₃ catalyst can be used for photocatalytic activity under visible light.

Chanjuan Xing et al. [27] synthesized various photo catalysts Cd_{1-x}Zn_xS (x = 0–0.92) using co-precipitation method and later on calcinated at 723K under N₂ atmosphere. Formation of a solid solution of Cd_{1-x}Zn_xS was indicated between ZnS and CdS by XRD patterns. As the value of x was decreased, UV-Vis spectra of Cd_{1-x}Zn_xS indicated a red-shift. Band gaps for photo catalyst were estimated between 2.20–3.12 eV (x =0–0.92) and showed an increase with an increase in value of x. Inner-irradiation type reactor was used for Hydrogen production. Maximum hydrogen evolution was observed in case of photo catalyst Cd_{0.62}Zn_{0.16}S.

1.7 Application of Solar Energy for Removal of Hazardous Chemicals In Water

The contribution of sunlight in expulsion of manufactured chemicals from environment is a well-documented field of research. Synthetic dyes that are being produced and consumed annually are not only source of environmental pollution but also causing serious health risks due to their toxicity [28].A lot different techniques such as activated carbon adsorption, oxidation by ozone (chemical treatment process),solvent extraction have been employed for removal of synthetic dyes but most often, all these results in

production of harmful by-products and considerable amounts of solid wastes which again, for proper disposal, require costly resources [29].

Keeping in view all these problems, Advance oxidation process (AOP) has recently been seen as an effective alternate for water purification [30] which is subcategorized into homogenous and heterogeneous catalysis. Heterogeneous catalysis has been successfully used for dye degradation. Titanium dioxide for being non-toxic yet in expensive and highly reactive has received great attention as photocatalyst and has been employed for environment clean-up [31-33]. Other than TiO_2 , large number of photocatalysts have been synthesized which were found effective for several organic dyes degradation and consequently environment clean up.

1.7.1 Photocatalytic Degradation of Organic Dyes

N. L. Olteanu et al. [34] synthesized Au-ZnO-SiO₂ photocatalyst by micro emulsion sol-gel method. This silica containing catalyst was categorized as mesoporous with decreasing surface area from Au-ZnO-SM>ZnO-SM>Au-SM>SM making it a better adsorbant material. Due to surface Plasmon gold absorption band, the capability of Au-SM and Au-ZnOSM to absorb light in VIS region was increased. A barrier was established between ZnO and Au nanoparticles, and on exciting it enabled a better transfer of electrons between ZnO and Au. This catalyst was used for the removal of Crystal Violet and Methylene Blue waste water by varying light irradiations. SiO₂ which was acting as the adsorption material, favored the interaction between ZnO, Au nanoparticles and as mentioned dyes.

A removal efficiency of 70 to 100 % was observed utilizing UV-VIS and sunlight by establishing continuous adsorption equilibriums and successive photo degradation process

Au-ZnO-SM may also be applied for the purification of waste water containing dye up to 60 mg/L with a removal efficiency of 100%.

K.Hayat et al. [35] synthesized ZnO nano particles with varying sizes using sol-gel method. Size of nanoparticles was varied by varying the calcination temperatures. It was observed that by increasing the calcination temperature, ZnO crystallites turned into agglomerates and lost their catalytic activity. ZnO nanoparticles synthesized using sol-gel method and 500°C as calcination temperature were found to be most effective for the photocatalytic degradation of phenol by its oxidation. Factors that effected the degradation process were concentration of phenol and catalyst, pH of solution and intensity of irradiation. ZnO nanoparticles calcinated at 500°C showed high photocatalytic activity because of smaller size, homogeneous and better dispersed NP.

Weifeng Yao and Jinhua Ye [36] reported highly crystalline CaBiVWO₈ and CaBiVMoO₈ structures, synthesized using solid-state method. The band gap values for both compounds CaBiVMoO₈ and CaBiVWO₈ were calculated to be 2.41 eV and 2.51, respectively. Both compounds were prepared using solid-state method. These photocatalysts were used for the decolorization of methylene blue that took place in a Pyrex glass tube while stirring constantly. Also, these materials showed good photo activity for O₂ evolution along with organic dye degradation. Reaction suspensions included 0.3 g of sample in 100 ml aqueous solution of Methylene Blue. Before the initiation of irradiation, suspensions were kept in dark conditions and magnetically stirred for 30 minutes to equilibrate adsorption/degradation. Using a UV-vis spectrophotometer and measuring absorbance at 656 nm, concentrations of MB solutions were calculated.

Jiade Lia et al. [37] synthesized Ag-based semiconductor which made use of visible light for photoactivity. High activity is observed for most of Ag-containing semiconductors. Factors that mainly effected the performance of catalyst were their crystal structures, morphological properties. Main drawback of Ag-based semiconductors is their photochemical corrosion. Other factors that reduced the photocatalytic activity of Ag-based catalysts included small specific area along with absence of a porous structure. By designing a hetero structure, coupling Ag-based semi-conductor with Carbon materials and by generating plasmonic effect, the photocatalytic activity and stability of catalyst could be enhanced. Furthermore, By modification in catalyst synthesis method,

highly porous structure and high specific surface area can be endowed by Ag-based semiconductors, which consequently enhances the photocatalytic activity. In addition, A particular morphology or special crystal facets in Ag-based semiconductors could also promote the photocatalytic behavior.

Wang et al. [38] synthesized Ag_3PO_4 NPs using precipitation/displacement method. It was observed that 97% of Methyl Orange could be degraded within an hour in presence of visible light and showed 2x activity than $\text{TiO}_2/\text{P25}$. Ag_3PO_4 spheroidal particles were synthesized by using precipitation method and the stability was investigated. The Ag_3PO_4 spheroidal particles were found highly. Photocatalytic activity showed no variation even after seven times of recycling.

Ke-Jian Ju et al. [39] synthesized Rambutan-like ZnO hierarchical hollow microspheres (ZnO HHMs) using hydrothermal route, and utilized carboxyl methyl starch (CMS) as template. The synthesized products were identified by using techniques such as X-ray diffraction (XRD), scanning electron microscopy (SEM), and transmission electron microscopy (TEM). Photocatalytic activity of catalyst was evaluated by extent of decolorization of Rhodamine B dye. CMS as template played an important role in formation of rambutan-like ZnO HHMs by preventing direct fusion of ZnO spheres during Ostwald ripening process.

Alireza Ejhieh et al. [40] did a study to compare the photocatalytic degradation ability of CuO-micronized zeolite X (CuO/MX) and zeolite X nano-particles (CuO/NX) for aqueous mixture of Methyl Orange (MO) and Methylene Blue (MB). Photocatalysts were identified and characterized by XRD, SEM, DRS, BET and FT-IR . The rate of photo decolorization was observed using UV-vis spectrophotometer. When results were studied, it was found that zeolitic beds play an crucial role in determining the photocatalytic activity of CuO semiconductors. CuO that has been supported on surface of Zeolite X nanocrystals showed much more photo activity towards Methyl Orange and Methylene Blue than unsupported CuO. It was also observed that Zeolite improves photocatalytic activity by preventing electron/hole recombination and prevents aggregation of CuO nanoparticles. Also, increased surface area of nano sized zeolite with

respect to micro sized zeolite increased the photocatalytic activity of CuO particles. Indicated results also highlighted the importance of pH on the photodecolorization of MO and MB dyes as it effects the charge on catalyst surface. Under given conditions, MO was degraded more than MB because of the thermonuclear structure of both dyes.

T.H.Nguyen et al. [41] prepared and characterized CuO/TiO₂ photocatalysts. Firstly, CuO nanocrystals were synthesized via thermal decomposition of Cu-oxalate at 400°C. Following this, CuO/TiO₂ core/shell nanocrystals were synthesized by hydrolysis of titanium isopropoxide (TIP) on CuO nanocrystal surface. Morphology of synthesized nanostructures was studied using scanning electron microscopy (SEM), and the crystal structure was determined by x-ray powder diffraction (XRD) and Raman spectroscopy. The size, shape and structure of synthesized nanocrystals was varied by varying the reaction time, reaction temperature and molar concentrations of precursor compounds. Increasing reaction time changed the shape of CuO structures from spherical nanoparticles to microspheres. One of the main advantage of newly synthesized CuO/TiO₂ core/shell structure is that it is resistant to photo corrosion.

A.Yousef et al. [42] doped CdO on ZnO nanofibers and studied its influence on photoluminescence properties of ZnO nanofibres. Nanofibres were of particular interest because of their long axial ratios which greatly modified the photocatalytic activity. CdO doped ZnO nanofibers were synthesized by preparing a sol gel that consisted of poly(vinyl alcohol), cadmium acetate and zinc acetate as precursors. This gel was then electrospun. It was also noted that calcination or change in Zn to Cd ratio did not affect the morphology of ZnO/CdO nanofibres. Addition of CdO to ZnO decreased the band gap due to which it could be utilized as photocatalyst in visible region. Indicated results showed that increasing CdO increased solid solubility. Nanofibres containing CdO content up to 39.4% by weight showed best photocatalytic activity among all prepared samples. Using this nanofibre, complete degradation of Methylene Blue dye was achieved within 4.5 h whereas longer time was required for complete dye degradation. Simplicity and low cost of synthesis scheme and requirement of solar radiation for initiation of photoreaction makes this class of nanofibers as suitable photocatalysts.

1.8 Simultaneous Production of Molecular Hydrogen (H₂) And Degradation of Dyes

Development of bi-functional photocatalysts capable of hydrogen production coupled with dye pollutant degradation has also been explored and numerous photocatalysts have been designed for this application.

Bing Cao et al. [43] synthesized a novel RuO₂/TiO₂/Pt photocatalyst by control-assembling TiO₂ hollow spheres with RuO₂ and Pt deposited onto outer and inner TiO₂ shell surfaces respectively. The as designed photocatalyst was used in simultaneous pollutant degradation and hydrogen evolution by employing photocatalytic oxidation and reduction. In this photocatalyst, RuO₂ acted for transfer of holes generated from TiO₂ which was followed by oxidation of organic pollutants for degradation. Similarly, Pt enhanced the transfer and deposition of electrons which in turn reduced proton to H₂ as cocatalyst. Thus the photocatalyst RuO₂/TiO₂/Pt showed a very high efficiency which was attributed to low electron/hole recombination, enhanced light harvesting due to multiple reflections in hollow TiO₂ chamber and synergetic effect between RuO₂ and Pt catalysts for photocatalytic oxidation and reduction.

Rajendran Kalyani and Karuppasamy Gurunathan [44] reported a PTh-rGO-TiO₂ photocatalyst synthesized via simple wet chemical method. In this photocatalyst, TiO₂ played an important role as photocatalyst along with rGO which acted as a good conductor and polythiophene having good hole conducting properties. This composite showed H₂ production at the rate of 214.08 μmolh^{-1} with a quantum efficiency of 14.17% at 400nm along with an effective degradation of methylene blue. Characterization and optical studies were made using XRD, UV, SEM, TEM, FTIR and Raman spectroscopy.

Hong Gao et al. [45] reported CuO₂ microcrystals as very efficient photocatalyst for the production of hydrogen as well as degradation of formaldehyde at room temperature utilizing MgO as sacrificial agent. It was also observed that other semiconductor catalysts such as TiO₂, ZnO, Bi₂O₃, Fe₂O₃ and CuO exhibited poor performance under the same

conditions. When detailed mechanism was studied, it was found that CuO_2 microcrystals showed reactivity in two ways; firstly by generating holes and electrons from CuO_2 which in turn generated hydrogen and hydroxyl ions. The hydroxyl radicals produced in reaction played important role in oxidizing formaldehyde and hydrogen evolution. Secondly, dissociation of Cu-O bond in CuO_2 resulted in the formation of $[\text{Cu}^+]$ ·paramagnetic which was also a principle factor for degradation of formaldehyde and H_2 production. It was also observed that Cu_2O microcrystals with {110} surface showed more hydrogen evolution activity than Cu_2O microcrystals with {111} surface.

Xi Wang et al. [46] synthesized a novel CdS-ZnS photocatalyst active under visible light. This heterogeneous photocatalyst was prepared using micro emulsion method carried in steps. The as synthesized nanoparticle composite was employed for the simultaneous generation of H_2 and degradation of organic pollutants under visible light. In this composite of ZnS-CdS, deposition of ZnS on CdS helped in suppressing electron/hole recombination which lead to more efficient H_2 production alongside improving the stability of ZnS-CdS photocatalyst as compared to bare CdS. It was also observed that when Ru catalyst was deposited on surface of composite, it increased the H_2 production upto 4 times. Along with hydrogen production, ZnS-CdS nanocomposite was found very efficient in degradation of organic substances including formic acid, methanol and ethanol. The highest rate of hydrogen production was estimated in case of CdS-ZnS-Ru photocatalyst at $266\text{mmol}/\text{m}^2\text{h}$ in formic acid solution with corresponding rate of organic degradation observed at $4272\text{ mg COD}/\text{m}^2\text{-h}$. The estimated energy conversion efficiency was found to be around 3.05% in visible region.

Similarly, Yasser A. Shaban [47] reported a carbon modified TiO_2 photocatalyst that was found effective for hydrogen production as well as for degradation of naphthalene in sea water. It was observed that modified TiO_2 not only showed photo activity under visible light but also showed a significantly increased photocatalytic activity. This increased photoactivity was attributed to carbon modification in bare TiO_2 catalyst. Favorable pH for simultaneous naphthalene degradation and hydrogen production was at 8 with an optical catalyst dose of $1.0\text{g}/\text{L}$ as indicated by experimental results.

Photocatalytic degradation of naphthalene using CM-n-TiO₂ photocatalyst was successfully described using Langmuir-Hinshelwood and pseudo-first order kinetic model.

Alexia Patsoura et al. [48] observed that degradation of organic compounds in un-aerated conditions lead to the production of CO₂ and in all cases CO₂ production was accompanied by H₂ production. The photocatalyst used for the studies was Pt-TiO₂ under UV and visible light conditions. It was observed that rate of hydrogen production was significantly increased in presence of organic additives. It was concluded that organic compounds acted as electron donors and scavengers of photo generated holes and oxygen leading to a decrease in e/h recombination in solution and consequently increasing hydrogen production rates. This process was assumed to continue until the complete oxidation of organic additive in solution which led to a steady-rate of H₂ production. The amount of CO₂ and H₂ produced directly depended on the nature of organic compound in solution and its initial concentration. This process was assumed environment friendly and cost effective as it led to the cleanup of water along with production of an efficient energy source.

1.9 Factors that Effect Photocatalytic Efficiency

There are a number of important factors needed to be considered in order to improve efficiency and productivity in case of photocatalysts. Factors that play an important role in influencing dye degradation process are initial concentration of dye and photocatalyst being used, pH of reaction mixture, particle size of photocatalyst, presence of electron acceptors, reaction temperature and light intensity.

.In this regard, several strategies have been employed to modify properties of semiconductor based photocatalysts such as band engineering to vary the band gaps and band positions of semiconductor photocatalysts. This variation in band gap has been found quite effective in order to improve photocatalytic efficiency and has been done employing a number of strategies such as doping. Quantum confinement effect, by

synthesizing solid solutions, sensitization of semiconductors and by hetero-structuralization of photocatalysts.

1.9.1 Co-catalyst Addition to Photocatalysts

For the development of an efficient semiconductor based photocatalyst, addition of a co-catalyst has been found as an effective strategy [49]. A reduction in electron/hole recombination leads to an increase in efficiency of photocatalyst. This enhanced efficiency is attributed to the lowering of the activation energy of reaction and catalyzing of surface reactions, that helps in trapping charge carriers and hence lower the electron-hole recombination.

TiO₂ photo catalyst efficiency strongly depends on the type of co-catalyst added [50]. In this regard, Platinum (Pt) has proved to be a good choice as it significantly increases the photo activity of TiO₂ catalyst for H₂ production [51]. Zn₂GeO₄ photocatalyst when loaded with noble metals shows greater efficiency with regard to water splitting process. It was observed that Zn₂GeO₄ catalyst with individual co catalyst showed relatively lower photocatalytic activity than that of dual co-catalyst load Zn₂GeO₄ [52].

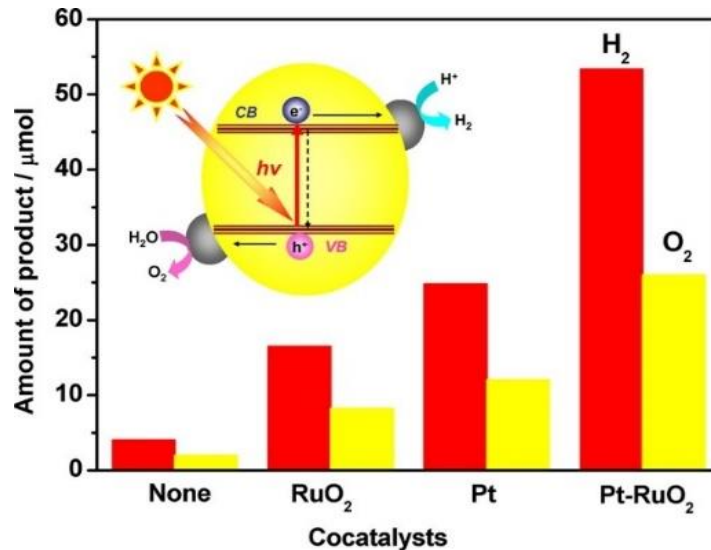


Figure 1.2: water splitting photo activity of ZnGeO₄ loaded with cocatalysts Pt and RuO₂ respectively [adapted from reference 52].

Addition of CoPi/Pt as oxidation/reduction cocatalyst to Bi_{0.5}Y_{0.5}VO₄ photocatalyst has shown enhanced photocatalytic H₂ evolution by addition of cocatalysts CoPi and Pt [53]. Domen and coworkers [54] observed a sufficient increase in water splitting activity when Rh/Cr₂O₃ and Mn₃O₄ nanoparticles were added as cocatalysts to GaN:ZnO.

1.10 ZnSe As a Semiconductor Photocatalyst

ZnSe is one of the first II-VI discovered semi-conductors which has found many useful applications in optical devices, light emitting devices (LED's), flat panel displays, lasers and transistors etc. ZnSe nanostructures have many potential applications in nanoscale electric and optical devices.

1.10.1 Potential Applications of ZnSe

1.10.1.1 LEDs

Low dimensional ZnSe nanostructures find their applications in a number of fields including sensors, lasers, photo catalysis, photodetectors, solar cells, field emitters, vivo imaging and light-emitting diodes (LEDs). Light emitting diodes (LED) have proved to be a promising alternative to fluorescent lamps and bulbs. ZnSe being a wide range

semiconductor, offers various applications in UV region of blue. Also doping changes intrinsic properties of ZnSe nanomaterials by changing their electronic states and facilitating electronic transitions in different energy levels.

Kwon et al. [55] synthesized Eu-capped ZnSe quantum dots using hot injection method with Eu-as precursor and utilized them for color-tunable emitters. A comparison between Zinc Selenide QDs, Eu capped ZnSe quantum dots and Eu based complexes revealed that nanocrystals with hybrid ZnSe-Eu capped structures exhibit bluish white light. Moreover, it was also observed that these Eu capped ZnSe showed 174% increased emission as compared to ZnSe quantum dots. Increased activity of these Eu capped was attributed to doping of Eu which in turn transferred energy to ZnSe quantum dots.

Furthermore, emission of white light is also an area of interest presently so, while keeping the energy efficiency, that photo metrically high quality white light can be generated. Sharma VK et al. [56] studied that ZnSe/Mn nanocrystals can be used as potential white light emitters without any toxicity and self-absorption issues. Shao et al [57] synthesized Mn doped ZnSe nanocrystals in aqueous medium employing microfluidic reactor. Emission of yellow light from Mn²⁺ ions and blue light from selenium sites resulted in emission of white light from nanocrystals. it was also observed that ZnSe and MnSe existed stably in zinc blend structure due to nearly equal lattice constants of both. A quantum yield of about 10.2% was achieved using this Mn:ZnSe quantum dots.

For this purpose, dispersion of nanoparticles in some conductive material such as semi conductive polymer results in formation of a bulk heterojunction which has several advantages including (1) simple synthesis process (2) production in large area [58]. Bulovic et al. [59] reported a novel solution based synthesis and study of Mn/ZnS and ZnSe/ZnS nanocrystals as AC-TFEL i.e. alternating current thin film electroluminescent devices with a yield of 65%. This AC-TFEL device was made by employing RF-magnetron spin casting and sputtering methods. It was observed that number of layers of

sputtered ZnS layers and their width played important role in determining efficiency of device.

Alternatively, Ji et al. [60] reported another method for blue QD-LEDs employing ZnSe/ZnS cores/shells QDs as emitters. Maximum luminance in this case was observed upto 1170 cd/m².

1.10.1.2 Lasers

ZnSe presents a great potential as ZnSe based lasers because of heavy anions present in ZnSe crystals with low energy optical photon cut off values which make them transparent in a wide range of optical spectra with decreased radioactive decay [61-63].

To date, visible light active semiconductor diodes consisting of wide band gap (mostly II–VI compounds) have been of great attraction great interest because of their cost effectiveness, high power and because of manufacturing ease [64,65].

1.10.1.3 Photodetectors

Photodetector or photo sensor is defined as an electrical and optical device in which the incidence of radiation causes a change in its electrical conductivity. When the energy of incident light is greater than the value of band gap of semiconductor being used, a change in number of electrons and holes takes place which in turn causes a change in electrical conductivity of that particular semiconductor [66-68]. There are several types of photodetectors that are used in various applications. For example, a photodiode consisting of a reversed biased operation. Another type is of photo resistors composed of semiconductors like CdS. They have the advantage of being cheaper but have slow response, low sensitivity and fairly strong non-linear response. Metal-semiconductor-metal (MSM) photodetector have two Schottky contacts. They are faster than several photodiodes having different band gaps. ZnSe (band gap value; 2.70 eV) has various applications as a part of opto-electronic devices.

1.10.1.4 Field Emitters

Field emission has its basis on phenomenon of quantum tunneling in which, under the influence of electric field, electrons are injected from material surface into vacuum [69,70]. field emitters find a number of applications in flat panel displays, microwave devices and high brightness electron sources [71]. ZnSe with work function of 4.84 eV is regarded as an excellent FE candidate compared to other materials

Wang et al [72] first studied FE pattern of ZnSe nanoribbon arrays. These nanoribbon arrays were synthesized using heating of ZnSe precursor. It was observed that after releasing ethylene diamine, morphology of nanoribbons was not affected and crystallinity of product was also improved. When a graph was plotted between applied electric field and FE current density, it was concluded that ZnSe nanoribbons are an excellent candidate for field emissions.

1.10.1.5 Sensors

(a) Humidity Sensors

Humidity sensors are defined as the electrical devices on which resistance or capacitance of sensor changes with change in humidity.it measures humidity in terms of relative humidity (RH). Choy and coworkers were the first to investigate ZnSe as resistance based RH sensors but the manufactured device lacked reproducibility [73]. Hu and coworkers [74] offered solution to these problems and synthesized ZnSe Nano rods by using molten hydroxide as reaction solvent without using any capping agent and dispersant. Relative resistance (R_{RH}/R_0), then measured, was between 20-80%.it was observed that as relative humidity was increased, resistance ratio decreased. Further results also indicated good stability and reproducibility of this humidity sensor.

(b) Gas Sensors

Gas sensors containing semiconductor nanomaterials have received gear attention due to better sensitivity than conventional thin films. Due to high surface to volume ratio, electrical transport properties of nanostructures can be altered effectively [75]. Park et al

[76] observed response of ZnSe nanowires when exposed to NO₂ in presence of UV-illumination and in dark. On exposure to NO₂, maximum resistance was observed and on removing NO₂, it recovered to initial value. An increase in sensing performance was observed when exposed to UV-illumination under room temperature.

Detection of gases using photoluminescence response has been a field of great interest recently because of fast sensing and easy reversibility of reaction along with distinction of gases. Hark et Al [77] observed photoluminescence response of different gases using ZnSe nanowires. Sensor based on this phenomenon showed an increased Near-Band-edge (NBE) in case of hydrogen gas while no NBE was observed on exposure to O₂, N₂ and air. Three different observations were made during time dependence of changes—firstly ZnSe nanowires instantly responded to the increase and decrease of hydrogen gas pressure, secondly a decrease in NBE intensity was observed in case of oxygen and argon which gradually increased on exposure to vacuum. Thirdly response to hydrogen, argon and nitrogen was found linear while that of oxygen was not. This difference in PL response could lead to the distinction in different gas species. Here reactive gases like hydrogen led to the change in surface state of nanowires with a resulting change in PL response of device and on the other hand, nonreactive gases like Ar and Nitrogen led to a decreased NBE emission.

1.10.1.6 Photocatalysis

Catalyst showing catalytic activity in presence of light energy is termed as photocatalyst. In photo catalysis, catalytic ability is measured in terms of a catalyst being able to generate electron-hole pairs. ZnSe, in this regard, has gained great importance in fields of catalysis, photochemistry and electrochemistry due to their significance in dealing with environmental problems like water and air pollution [78]. Yao et al. [79] demonstrated through experimentation that ultrathin ZnSe rods showed enhanced performance when compared with conventional nanorods in photo degradation of Methyl orange. Increased

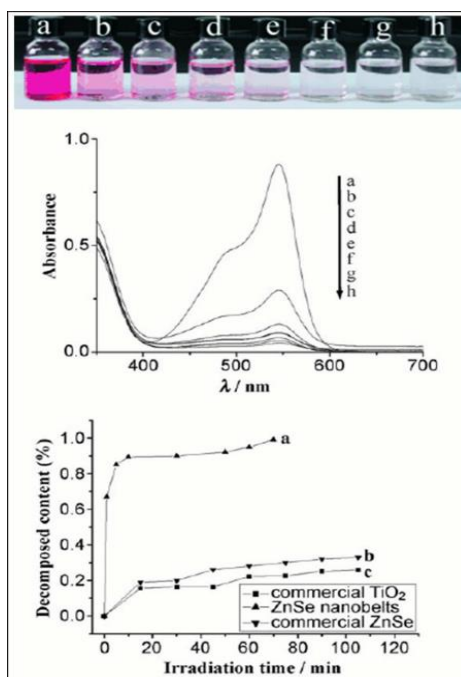


Figure 1.3: fuchsine acid solution (color changes and absorption spectra) in the presence of ZnSe nanobelts under exposure to UV light: a) initially prepared solution; b–h) solutions after adding ZnSe nanobelts [Adapted from reference 80].

activity was attributed to charge carriers and large specific surface area. Xiong et al. [80] observed increased photo degradation rate in case of ZnSe nanobelts than commercial TiO₂ and ZnSe, all exposed to same UV irradiation. During experimentation, photocatalytic degradation mechanism of fuchsine acid was observed for all three photocatalysts. It was noted that in case of ZnSe nanoparticles, characteristic peak of fuchsine acid at 545 nm diminished sharply which completely disappeared after exposure of fuchsine acid to UV irradiation for 70 min.

Generally, variation in reaction conditions can lead to change in size shape and properties of final semiconductor product which are important for their industrial properties. 3D wurtzite ZnSe structures were found effective in photo degradation of methylene blue and ethyl violet aqueous solution when exposed to UV irradiation and showed increased photocatalytic activity than P25 and ZnSe microspheres. It was also observed that ZnSe nanotubes array can provide solutions towards the problems of recovery and stability which was absent in case of typical powder form photocatalysts.

1.10.1.7 Doped Semiconductors

(a) Solar Cells

An electrical device that, by photovoltaic effect, converts light energy directly into electrical energy is termed photovoltaic cell or solar cell [81,82]. when light energy falls on this photoelectric device, its electrical properties such as voltage, current and resistance changes therefore, on exposure to solar energy, these cells can generate electrical response without any attachment to external voltage source. ZnSe has been extensively used as solar based device.

Use of nanostructures in solar cell devices offer several advantages such as formation of vertical radial junction and trapping of light with reduced reflection. It is also seen that nanoparticles properties can be altered when nanostructures are small enough for application of quantum effects. Another advantage offered is lower cost required for synthesis of such nanostructures [83,84].

1.10.1.8 Vivo Imaging

biomedical fluorescent imaging has recently attracted great importance [85]. Ability of bi-functionalized quantum dots in labelling of cells have made possible the extended cell visualization. moreover, under continuous illumination, multicolor florescent imaging has also been made possible [86]. In vivo research refers to the experimentation done in living bodies of experimental organism [87,88]. By changing band gap of semiconductors nanoparticles, new materials with different properties and consequently new applications

can be synthesized [89]. Charvet et al. [90] synthesized CdS/ZnSe core/shell nanocrystals that were found very effective in fluorescent biological labeling nerve cells.

Chapter 2

Experimental and Characterization Techniques

2.1 Chemicals

All chemicals for ZnSe nanoparticles synthesis were of analytical grade and used without any further purification. Deionized water was used for all preparations. List of all chemicals used are given in table

Table2.1 : List of chemicals for synthesis of ZnSe nanoparticles.

Sr. No.	Chemical	Chemical Formula	Molar Mass(g/mole)	%age Purity(%)	Vendor
1	Zinc Acetate	$Zn(H_3CCOO)_2 \cdot 2H_2O$	219.50	99-100	Riedel-de Haen
2	Selenium powder	Se	78.96	99.5	Merck
3	Potassium Hydroxide	KOH	56.106	85-100	Sigma Aldrich
4	Hydrazine Hydrate	N_2H_4	32.05	80	Merck

2.2 Synthesis of Nanoparticles

There are several methods that have been reported for nanoparticle synthesis. Synthesis of nanomaterials has been a dynamic field and many chemical and biological processes have been employed. Chemical processes include mechanical attrition, chemical vapor synthesis, Sol-Gel technique, gas condensation, chemical precipitation, ionized cluster beam, electrodeposition, liquid metal ion source, molecular beam epitaxy, sputtering and gas aggregation of monomers reaction in micro emulsions and auto combustion, hydrothermal route and chemical precipitation in presence of capping agents. Biological processes include using, enzymes, fungus, microorganisms and plants and/or plant extracts [91-96].

2.2.1 Gas Condensation

In this procedure, metallic or inorganic material is vaporized via thermal evaporation in 1-50m atmospheric pressure. During gas evaporation, ultra-fine particles with dimensions of around 100nm are formed by gas phase collision because of high residual gas pressure. Gas pressure required is >3 mPa. Gas vaporization sources can be resistive heating, high or low energy electron beam and induced heating. Clusters are formed due to homogenous nucleation. This whole system is fitted with an ultra-high vacuum (UHV) evaporation system, compaction device and liquid nitrogen filled scrapper assembly. After synthesis, nanoparticles are collected by scrapping and evaporation is done [97]. Apart from being slow, this method has disadvantages of temperature ranges, source-precursor incompatibility and different evaporation rates in an alloy. Over the years, alternative sources such as Iron (Fe) is being evaporated in an inert gas such as He where Fe nanocrystals condense as loose powder. Laser evaporation or sputtering is also being used [98]. Sputtering is a method in which atoms present on the surface are launched out from surface by bombarding an energetic atomic or molecular size specie. This technique uses low pressure environment to produce a number of ultrafine particles such as Ag, Fe and Si. sputtering electron beam heating and plasma methods are also employed for synthesis purposes.

2.2.2 Vacuum Deposition and Vaporization

In this method, elements and compounds are first vaporized and then deposited in presence of vacuum. Materials are vaporized using thermal methods carried out at a pressure of < 0.1 Pa or 1m Torr and vacuum of 10 – 0.1 MPa. Temperature range of substrate is from room temperature to 500°C. By keeping rate of vaporization high, good deposition rates can be obtained. It was observed that very useful deposition rates were obtained at v.p. of 0.01 torr. Nucleation occurs as a result of multibody collisions. Size of particles ranges from 1 – 100 nm and are named as clusters or ultrafine particles [99-101]. Vacuum deposition process is advantageous with respect to high deposition rates and economic point of view but depositing many compounds is rather difficult.

2.2.3 Chemical Vapor Deposition (CVD) and Chemical Vapor Condensation (CVC)

In chemical vapor deposition method, a solid sample is placed on a heated surface through a chemical reaction from vapor or gas phase. CVC reaction requires certain activation energy which can be supplied by a number of methods. A thermal CVD reaction initiates above 900°C temperature. Usually reaction apparatus consists of deposition chamber, gas supply system and an exhaust system. In laser CVD substrate molecules break down under the effect of laser thermal energy while in photo-laser CVD, UV radiations with sufficient photon energy cause pyrolysis of chemical bonds and later deposition occurs at room temperature. Different nanocomposites like SiC/Si₃N powder was synthesized using H₂ as gas source at 1400°C.

In 1994, another method of chemical vapor condensation was developed in which vapors from metal organic precursors undergo pyrolysis in reduced atmospheric pressure. Employing CVD method, ZrO₂, Y₂O₃ and Nano whiskers have been synthesized [99-102]. Yield of reaction can be increased by increasing diameter of reactor walls and by controlling mass of fluid passing through reactor.

2.2.4. Mechanical Attrition

Mechanical attrition results in formation of nanostructures by decomposition of scratchy grained structure because of plastic deformation. β -SiC and Al powders had been

synthesized using high energy ball mill. Moreover, ceramic and ceramic nanocomposites such as WC-14% MgO has also been synthesized recently. Rod milling and ball milling techniques has been an attractive mechanical alloying process for synthesis of new materials. This mechanical alloying process can easily be carried out at ambient temperature using centrifugal type mills, vibratory mills, low energy mills and high energy mills [103,104].

2.2.5 Chemical Precipitation

During the process of chemical precipitation method, size of nanoparticles is controlled by arrested precipitation. In this case, thermal coagulation and Ostwald ripening was evaded by double-layer repulsion of crystallites at low temperatures using non-aqueous solvents. To avoid agglomeration, surfactant is added. Obtained product is then centrifuged, washed and vacuum dried [102-104].

2.2.6 Sol-Gel Techniques

Along with aforementioned techniques, sol-gel process is a well-known method used for synthesis of nanoparticles. Process involves formation of a sol-gel where ‘sol’ indicates a colloidal suspension and ‘gel’ is the gelatinous network in liquid phase. Precursors used for synthesis of collides are metal alkoxide and aloxysilans ions such as tetraethoxysilane (TEOS) and tetramethyloxysilane (TMOS) forming the gels. A sol-gel process inculcates the formation of homogenous solution of aloxides which serve as a precursor for the synthesis alumina, titania and silica along with others [105-108] for initiation of reaction with a controlled pH, catalyst is required. Sol-gel formation takes place in four basic steps:

1. Hydrolysis
2. Condensation
3. Particle growth
4. Particle agglomeration

During the first step of hydrolysis, [OH-] groups are replaced by [OR] group. Reaction can be accelerated by addition HCl and NH₃ as catalyst. Process

continues until the complete replacement of alkoxy groups by hydroxyl ions followed by condensation and formation of siloxane bonds along with water and alcohol.

Condensation step involves formation of siloxane bond either by production of water or alcohol. Hydrolysis rate is varied by variation in pH, molar ratio and reagent concentration along with ageing and drying. Structure and properties of sol-gel can be changed by changing these parameters.

During the growth and agglomeration step, siloxane bonds increase in number forming a network which consequently gives gel on drying. Spherical nanoparticles are formed at $\text{pH} > 7$.

2.2.7 Electrodeposition

Nanomaterials are produced using electrodeposition method. Uniform and mechanically strong films are obtained as a result of this process. Recent advancements in this field have resulted in form of several non-traditional methods that have been put in use for synthesis and deposition of nanoparticles. Properties such as resistance and hardness are affected greatly by particle size and an increase in these properties can lead to a far better coating performance [109,110].

2.2.8 Hydrothermal Process

Hydrothermal process is an effective and efficient process for synthesis of nanoparticles. This process involves the use of a steel lined autoclave at high temperature and pressure conditions. When a chemical reaction is performed using a solvent, it is referred to as solvothermal process. However, a reaction performed using water as a solvent in autoclave is known as hydrothermal process. High temperature and pressure conditions provide opportunity for solubility of inorganic chemical compounds in solvent which would remain undissolved otherwise. To increase the reaction kinetics, the electric, ultrasonic and microwave fields can be introduced in system. Several inorganic materials have been synthesized using this process.

2.3 Sample preparation

For ZnSe nanoparticles synthesis, hydrothermal method was employed. Initially in the synthesis process, 0.1M zinc acetate and 0.1M selenium powder was dissolved in a 6M KOH solution. Hydrazine hydrate (2ml) was added to the mixture which was later on stirred for 1 hour at ambient temperature. The mixture was then transferred to 50ml Teflon lined autoclave and placed in oven for 3 hours at 200°C.

Table 2.2 ZnSe Synthesized by Changing Reaction Temperatures					
Sample no.	Zinc Acetate(M)	Se-powder(M)	KOH(M)	Temperature(°C)	Reaction time(Hrs)
1	0.1	0.1	6	120	3
2	0.1	0.1	6	140	3
3	0.1	0.1	6	160	3
4	0.1	0.1	6	180	3
5	0.1	0.1	6	200	3
ZnSe Synthesized by Changing KOH Concentration					
Sample no.	Zinc Acetate(M)	Se-powder(M)	KOH(M)	Temperature(°C)	Reaction time(Hrs)
6	0.1	0.1	2	200	3
7	0.1	0.1	3	200	3
8	0.1	0.1	4	200	3
9	0.1	0.1	5	200	3
10	0.1	0.1	6	200	3
ZnSe Synthesized by Changing Reaction Time					
Sample no.	Zinc Acetate(M)	Se-powder(M)	KOH(M)	Temperature(°C)	Reaction time(Hrs)
11	0.1	0.1	6	200	1
12	0.1	0.1	6	200	3
13	0.1	0.1	6	200	5
14	0.1	0.1	6	200	7
15	0.1	0.1	6	200	9

After the autoclave has been cooled, yellow precipitates are collected, washed with deionized water several times and finally with ethanol. Drying of precipitates was done at 75°C for 7 hours. Obtained ZnSe nanoparticles were grinded to fine powder and stored for further characterization and analysis. Same reaction was repeated for different KOH concentrations (2M, 3M, 4M, 5M), for different reaction temperatures

(120°C,140°C,160°C,180°C) and finally with different reaction time (2 hrs,5hrs,7hrs,9hrs) while keeping all the other reaction conditions constant. Samples being prepared are mentioned in table 2.3 along with their compositions

2.4 ZnSe Modification with Pt and Activity Tests

A disadvantage of semiconductor based photocatalyst is that electrons and holes generated during the photoexcitation can recombine on surface of photocatalyst and consequently reduce the photocatalyst efficiency. In the synthesized ZnSe photocatalyst, to suppress the e/h recombination, the photocatalyst was modified by incorporating 1% wt. Platinum metal on surface of photocatalyst. In a typical experimental arrangement, H₂ production and degradation of desired organic compound was performed at ambient temperature (25°C) in a reactor with 0.05 g of photocatalyst and 50ml aqueous solution with desired amount of an organic pollutant. Organic pollutants in this case were methanol and sodium sulphide which are generally released from industries such as paper and pulp, textile industries and also as a result of volcanic activities. The reactor was a 100 cm³ double jacket quartz glass reactor. Argon gas was purged through the reactor and ZnSe/Pt suspension at a constant flow rate of 10 cm³ /min to remove any traces of atmospheric oxygen. Glass reactor was connected to a quadrupole mass spectrometer in which the actual inlet gas flow rate was 1 cm³/minute. Before the start of experiment, the reactor was kept in dark for one hour to obtain a stable baseline. Photocatalytic measurements were carried out using Osram XBO 1000 watt Xenon Arc Lamp in a Müller LAX 1000 Lamp placement for 4-15 hours.

2.5 Characterization Techniques:

Characterization techniques used for as synthesized ZnSe nanoparticles were as follows:

1. X-ray diffraction crystallography (XRD)
2. Scanning Electron Microscopy (SEM)
3. UV-Visible Spectrophotometry (UV-Vis)

4. Transmission electron microscopy (TEM)
5. Energy Dispersive X-ray Spectrometry (EDX)

2.5.1 X-ray Diffraction Crystallography:

The basic principle of X-ray Diffraction involves the application of an x-ray on the material under consideration. The x-rays, after interacting with electrons in material, scatter in different directions. If the wavelength of x-rays being scattered is comparable to spacing between atoms then a constructive interference occurs and a pattern is obtained on screen.

Basic apparatus in an X-ray diffractometer consists of three parts including **(1)** X-ray tube for generation of x-rays. X-rays are generated inside the tube by heating and acceleration of electrons. Electrons with enough energy to knock out inner electrons of materials produce characteristic x-rays. **(2)** A sample holder containing sample. These generated x-rays are then directed to sample holder containing the sample. Intensity of x-rays is recorded as sample and recorder is rotated. X-rays which satisfy the Bragg's equation after impinging sample results in constructive interference and results in a pattern on screen after passing through the detector. **(3)** A detector helps to record and process the obtained signal and sends it to an output device such as a computer screen.

X-ray diffraction is an important quite conventional technique used for determining crystallographic structure and morphology. An increase and decrease in intensity of XRD peak can be seen according to an increase and decrease in quantity of constituent material. This technique gives an insight to the translational symmetry, size and shape of unit cell and also gives information about the electron density inside a unit cell. Using the peak intensities, we can find where the atoms positions are. Crystallite size is calculated using Scherrer equation which is given as $CS = k \lambda / \beta \cos \theta$ where

CS = crystallite size constant

[K] = 0.94 full width at half maximum (FWHM)

β = FWHM $\times \pi/180$

$\cos \theta =$ Bragg's equation.

2.5.2 Scanning Electron Microscope

Scanning electron microscopy or SEM is used to determine the size, shape and morphologies of synthesized nanoparticles. It gives high resolution images for the surface of a sample under consideration. SEM has the same working principle as that of optical microscope but utilizes scattered electrons from the sample rather than photon. In SEM, signals are generated by interaction of electrons with sample under study. Electrons commonly associated with imaging of sample are secondary electrons and backscattered electrons. Former helps in determining morphology and topology while latter help in determining phase structure of sample being examined. The interaction of electron beam and sample generates different signals which provides information about structure, morphology and surface characteristics. Due to acceleration of electrons caused by applied electric potential, wavelength is shorter than that of photon which makes able the Scanning electron microscopy sensitivite is down to 1 nm [111]. All SEMs instruments include same basic components namely (1) An electron source gun (2) Lenses (3) Sample stage (4) Detectors and (5) Data output devices.

2.5.3 UV-Vis Absorbance Spectroscopy

UV-Vis spectrophotometry is used for the measurement of optical properties of a given solution. A ray of light is passed through the sample under consideration and then the quantity of absorbed light is measured. With varying wavelengths, absorbance is measured at each wavelength and this measured absorbance can be used to find the concentration of solution employing Beer-Lambert law. The optical properties of nanoparticles are sensitive to concentration, size, shape, agglomeration rate and refractive indexes of nanoparticles near surface. This makes UV/Vis an important tool for identification and characterization of nanoparticles. Nanoparticles of metals such as silver and gold interact strongly with some specified wavelengths. These optical properties are the fundamentals of the field of plasmonics.

2.5.4 Transmission Electron Microscopy (TEM)

Transmission electron microscopy follows the same principle as that of light microscopy. But because of lower wavelength from electron source, resolution, in case of TEM, is thousand times better than light microscopy. Transmission electron microscopy involves the use of an electron beam which is passed through an ultra-thin sample under consideration. Electrons are transmitted through the sample as they pass interacting with the sample. An image is obtained as transmitted electron beam interacts with the specimen which is, later on focused and magnified on a layer of photographic film, fluorescent screen or can be detected using a sensor like CCD camera. TEM is widely used for structural compositional analysis. Transmission electron microscopy is a major analysis method used in nanotechnology, pollution, materials sciences, virology and cancer research.

2.5.5 Energy Dispersive X-ray Spectrometry

EDS/EDX makes use of the X-ray spectrum obtained by bombarding electron beam on a solid sample to get a localized chemical analysis. Elements from Beryllium (4) to Uranium (92) can be detected generally but certain light instruments are not capable of detecting below atomic number 10. Qualitative analysis is simpler in the terms that it gives straight forward spectrum lines while Quantitative analysis shows spectrum lines relative to concentration of each element present and with calibration standards of known composition. By scanning electron beam in a raster with reference to peak intensities, element distribution maps can be obtained. These collected images show surface topography or mean atomic mass difference.

Chapter 3

Results and Discussion

This chapter includes the detailed results of synthesis, characterization, optical and photoluminescence properties of the nanostructured ZnSe and ZnSe/Pt photocatalysts.

3.1 Effect of Reaction Conditions on ZnSe

On changing different reaction conditions like reaction time, temperature, KOH concentration, change in phase structure, morphology and size of particles was observed.

3.1.1 Effect of Temperature

Figure 3.1 shows XRD patterns of ZnSe samples prepared at 120°C, 140°C, 160°C and 180°C without any change in other reaction conditions. The analysis was performed using Bruker D8 focus diffractometer with Ni-filtered Cu-K α radiations. All hkl values of (111), (220), (311), (400), (331) referred to cubic zinc blende structure of ZnSe (JCPDS no. 00-037-1463) where a=b=c= 5.6 Å. At high reaction temperature, X-ray diffraction peaks become far more narrower and higher indicating an increase in crystallinity of final product. This can be correlated with Debye-Sherrer's equation which indicates that peak width is inversely proportional to the crystallite size

$$CS = k \lambda / \beta \cos \theta \quad (1)$$

In figure 3.1, it can be seen that as the temperature is increased from 120°C to 160°C and then 180°C stepwise, peaks width increases indicating a decrease in particle size in an order of 19.8 nm, 17nm, 12nm, 9nm respectively. One reason for broadening of peaks can be that number of diffraction planes reduces with decrease in particles size which

ultimately leads to broadening of peaks [112]. Sample prepared at 180°C showed some extra peaks in XRD indicating that agglomerates of ZnSe at this temperature were of low purity. While in case of reaction temperature of 200°C, XRD peaks obtained are narrow and intense implying a large particle size (30nm). It indicates that Sample prepared at 200°C shows highest crystallinity as compared to other prepared samples therefore, this reaction temperature was used for synthesis of an optimized sample of ZnSe for further studies.

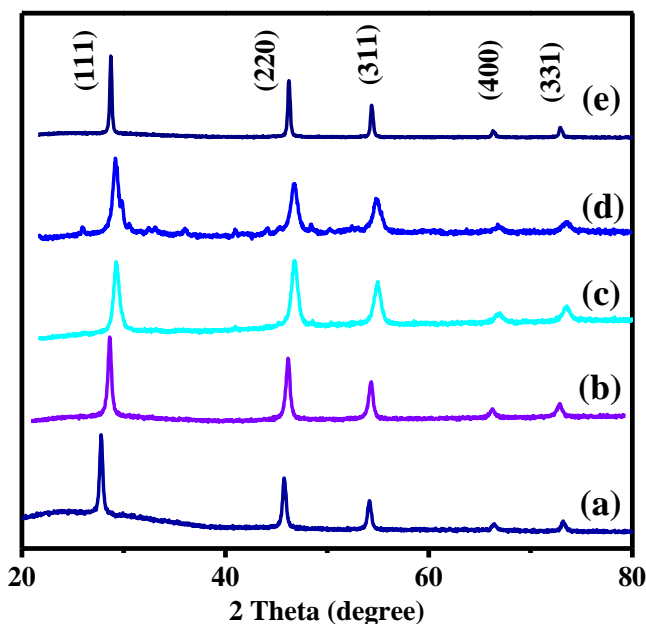


Figure 3.1: XRD patterns of ZnSe samples obtained at (a) 120°C, (b) 140°C, (c) 160°C, (d) 180°C, (e) 200°C

For morphology studies, Scanning electron microscopy (SEM) was performed. Figure 3.2 shows SEM images for samples of ZnSe nanostructures obtained at reaction temperatures 120°C, 140°C, 160°C and 180°C and 200°C without any other reaction condition changed. Images show that most of the product obtained is comprised of ZnSe cubic nanoparticles. Figure 3 (a) shows ZnSe structures obtained at 120°C. No well-defined ZnSe nanostructures can be observed at this temperature. As temperature is increased from 120°C to 140°C, 160°C and 180°C and then to 200°C, more uniform ZnSe

nanoparticles are obtained at higher temperatures. (120°C ,140°C ,160°C). Favorable crystallinity at higher temperatures implies to the fact that sufficient activation energy was available at higher temperatures favoring more crystalline and uniform structure formation.

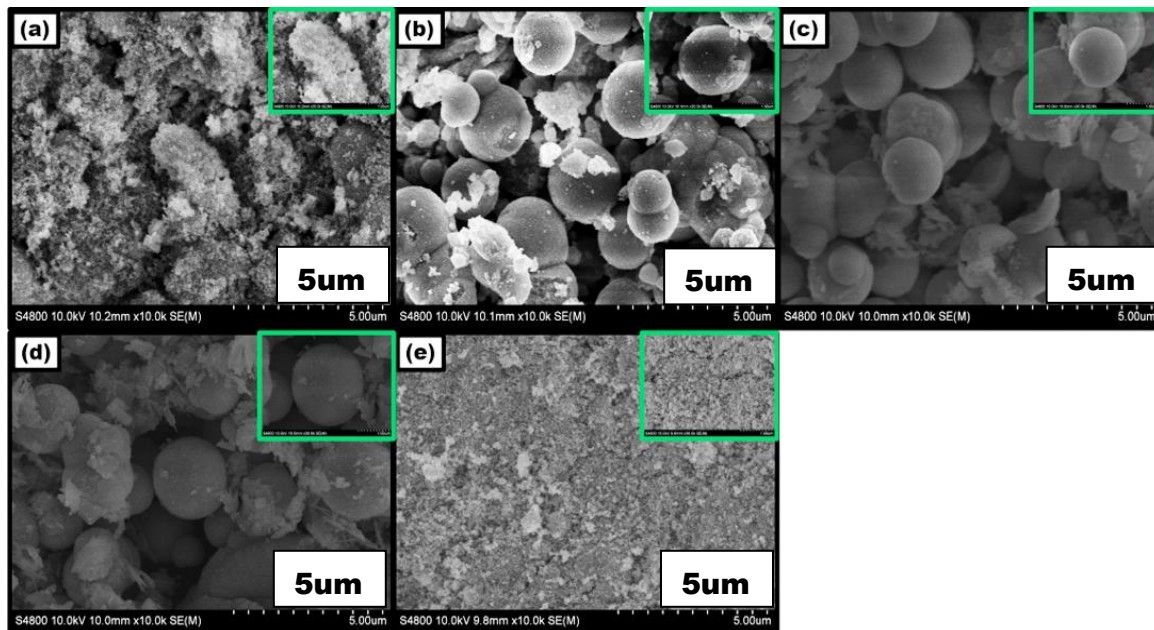


Figure 3.2: SEM images of ZnSe microspheres at (a) 120 °C, (b) 140 °C, (c) 160 °C, (d) 180 °C and (e) 200 °C

ZnSe nanocrystals at surface gradually develops into cubic structure as hydrothermal reaction temperature is increased. The reason for well-defined microspheres at elevated temperatures may be that at higher temperatures there is more thermal energy available for growth of ZnSe nanocrystals. As surface energy of spherical particles is more than cubic particles therefore more spherical particles can be seen at lower temperatures as shown in Fig. 3.2 (a). With increasing hydrothermal reaction time,an intense temperature field is experienced which breaks nanostructures into nanoparticles of smaller size as shown in Fig. 3.2 (e).

3.1.2. Effect of KOH Concentration

The effect of KOH concentration on morphology and particle size of final product was also investigated further. Concentration of KOH was gradually increased from 2M, 3M,

4M, 5M to 6M. Figure 3.3 shows the peak widths decrease with increase in pH of solution. Least crystallinity was observed in case of KOH concentration of 2M, while highest crystallinity and particle size observed in case of 6M. Figure 3.3 shows XRD patterns of products prepared at 200°C and reaction time of 3h while using different concentrations of KOH (2M, 3M, 4M, 5M and 6M). Here increasing KOH concentration resulted in narrow and sharp peaks indicating an increase in product crystallinity. Highly crystalline product being obtained at KOH molar concentration of 6. Using Debye-Scherrer equation, calculated crystallite sizes were found in a range of 14.9 nm, 18.5 nm, 20.8 nm, 25.8 nm and 30.4 nm for KOH concentration of 2M, 3M, 4M, 5M and 6M respectively. Increase in particle size is due to agglomeration of particles in sample

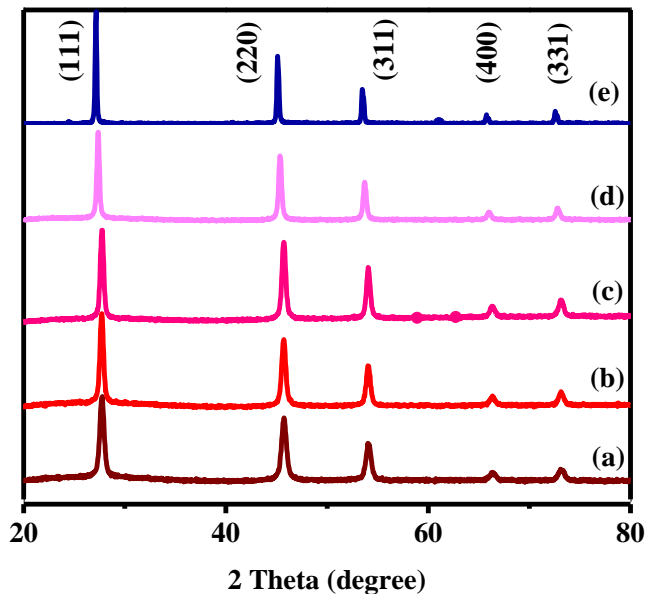


Figure 3.3: XRD patterns for as-synthesized ZnSe nanoparticles at KOH conc. Of (a)2M, (b)3M, (c)4M, (d)5M, (e)6M.

Figure 3.4 shows SEM images for ZnSe microspheres obtained with KOH concentrations of 2M, 3M, 4M, 5M and 6M KOH. Previous studies have revealed that spherical particles could not be synthesized without presence of KOH or NaOH [113]. At lower

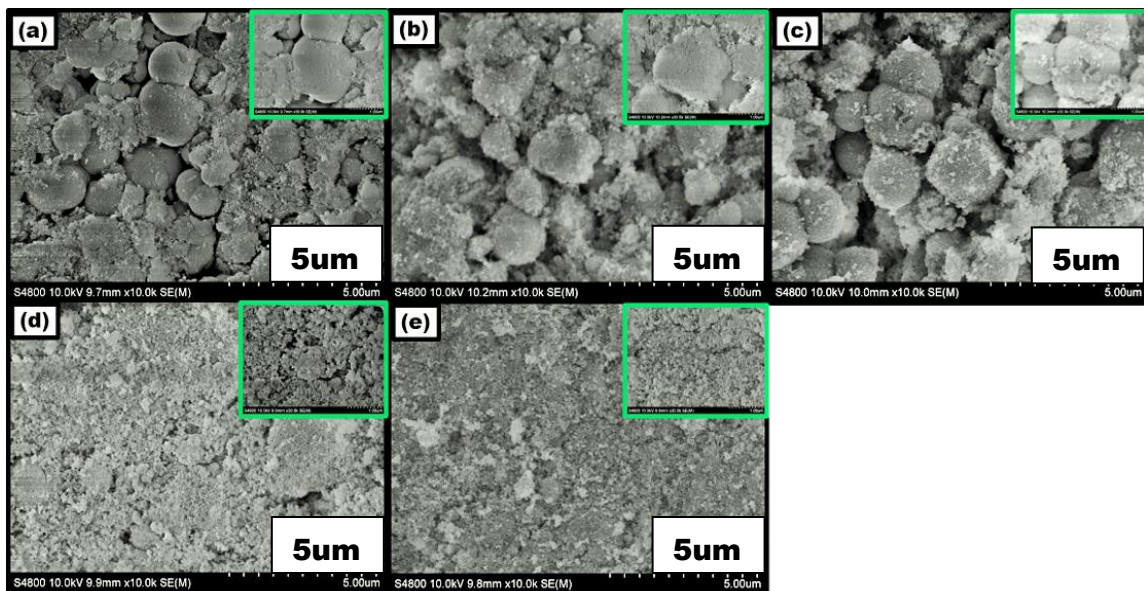


Figure 3.4: SEM images for ZnSe synthesized using KOH (a) 2M, (b) 3M, (c) 4M (d) 5M, (e) 6M concentrations of KOH, agglomerated nanoparticles can be observed and as concentration is increased, uniform small sized ZnSe nanoparticles are obtained. Presence of KOH in sample affects the pH of solution which in turn affects the particle size and morphology of product. By changing KOH concentration from 2M to 6M step-wise, nanoparticles become spherical and more uniform.

3.1.3. Effect of Reaction Time

Another parameter measured for size, morphological studies of ZnSe nanoparticles was reaction time. Figure 3.5 shows XRD patterns of products being obtained at different reaction temperatures ranging from 1, 3, 5, 7 and 9 hours with constant conc. Of KOH (6M) and reaction temperature (200°C). All XRD peaks corresponded to cubic blende structure ZnSe. In figure 3.5, it can be seen that, except for reaction time of 1 hour, all other XRD peaks are narrow and intense, indicating a high crystallinity of product. When crystallite size is calculated using Debye-Scherrer's equation for reaction time of 1 hour, 3 hours, 5 hours, 7 hours and 9 hours, it was 8.05 nm, 30.4 nm, 29.4 nm, 31.5 nm and 30 nm respectively. The reason for small crystallite size in case of 1 hour can be explained by the fact that, as Ostwald ripening process is the main phenomenon involved here,

therefore, less time of reaction led to least nucleation and hence small crystallite size. While in case of other reaction times of 3,5,7 and 9 hours, there was enough time for initially formed nanoparticles to aggregate and lower the surface energy of nanoparticles by aggregation. It can also be inferred from crystallite size calculation that reaction time of 3,5,7 and 9 hours had no significant effect on particle size and resulted in almost same degree of crystallinity in product.

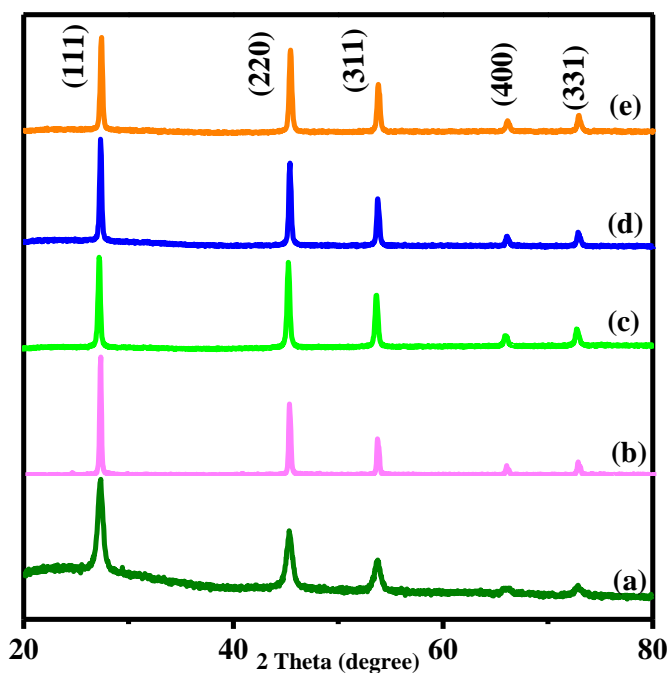


Figure 3.5: XRD patterns of ZnSe nanoparticles synthesized at reaction times (a)1 h, (b)3h, (c)5h, (d)7h, (e) 9h

Figure 3.6 shows SEM images for products obtained with reaction time 1h, 3h, 5h, 7h and 9h. It can be seen that there is a little change in morphology and size of nanoparticles with change in reaction time. As reaction time is increased from 3h to 7h and then 9h, agglomeration of nanoparticles can be seen. Despite no significant change in morphology of nanoparticles, it can be seen that for reaction time of 5,7 and 9 hours, nanoparticles are

forming aggregates with unclear boundaries giving an overall rough appearance to sample.

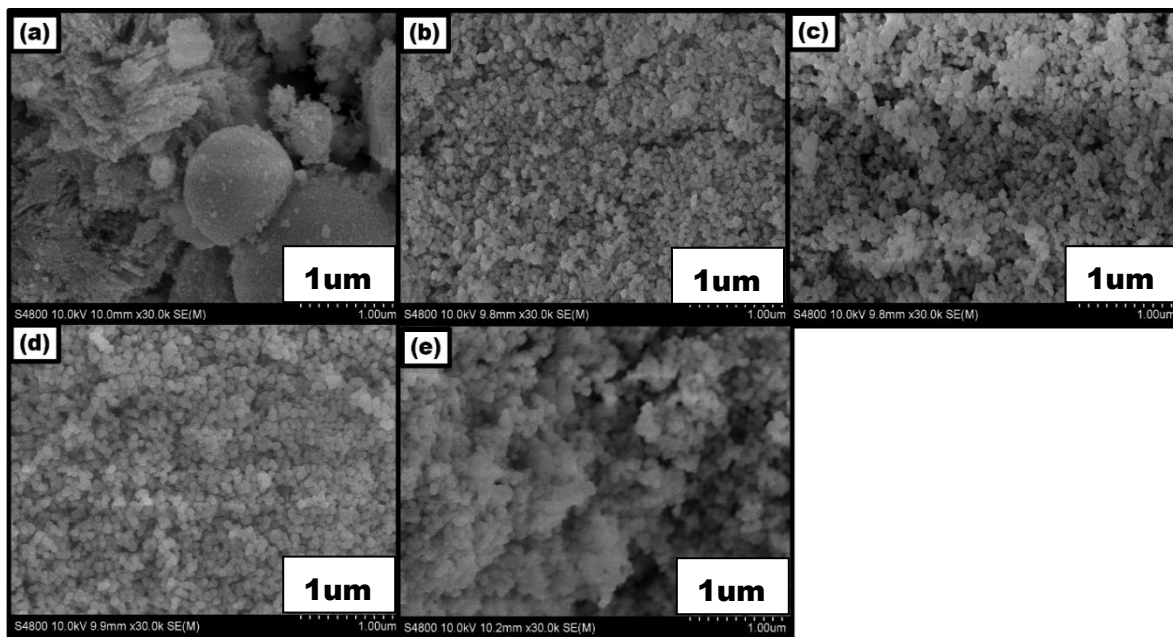


Figure 3.6 SEM images of ZnSe nanoparticles synthesized at reaction temperature of (a) 1h, (b) 3h (c) 5h (d) 7h, (e) 9h

Therefore, 3 hours was chosen as a suitable reaction time for preparation of ZnSe sample further investigated for photocatalytic activity.

To add all up, hydrothermal reaction time has least effect on the particle size and lesser effect on morphology of obtained products.

3.2 Phase and Morphological Results for ZnSe, ZnSe/Pt

The optimized ZnSe nanoparticles sample was prepared using optimized conditions and investigated using XRD. Figure 3.7 shows a typical XRD pattern of ZnSe nanostructures prepared by using hydrothermal route. All diffraction peaks can be referred to cubic ZnSe crystal structure and match with standard pattern (00-037-1463) which confirm synthesis of single phase ZnSe with cubic crystal system. XRD patterns showed a strong

orientation along (111) direction. The lattice parameters for ZB are $a=b=c=5.67 \text{ \AA}$ (space group =F-43m). Calculated cell volume was 176.2 cm^3 which was close to value stated in

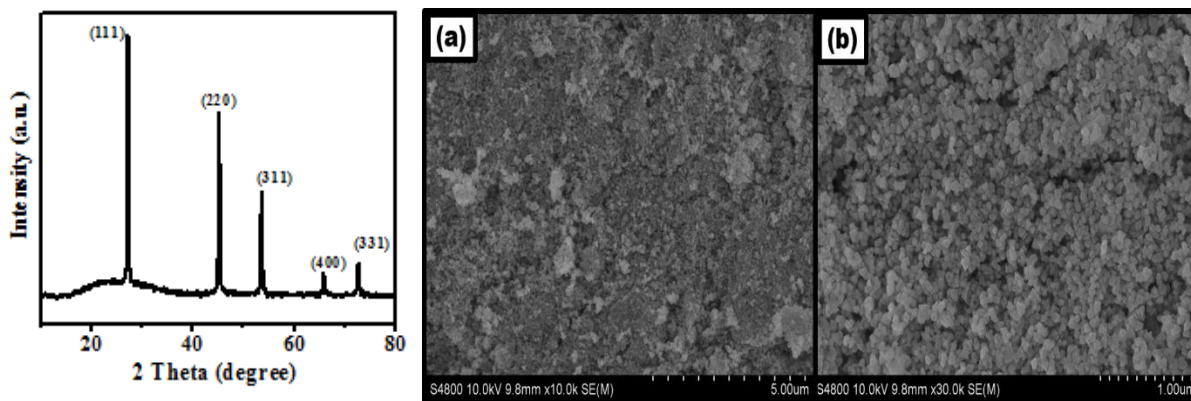


Figure 3.7: XRD and SEM patterns of ZnSe photocatalyst using 6M KOH solution and hydrazine hydrate at $200 \text{ }^\circ\text{C}$ for 3 h.

literature (182 cm^3). The matching of all peaks show that synthesized sample is free of any impurity.

3.3 Optical Analysis

The optical properties of samples are evaluated using UV-visible spectroscopy. UV-visible spectra obtained for ZnSe nanoparticles are shown in figure 3.8. Two absorption peaks are observed at approximately near 475 nm and 575 nm. The first absorption can be refers to bulk band emission of ZnSe while the other one is probably due to self-activated luminescence or surface emission or due to some donor-acceptor pairs related to band gap

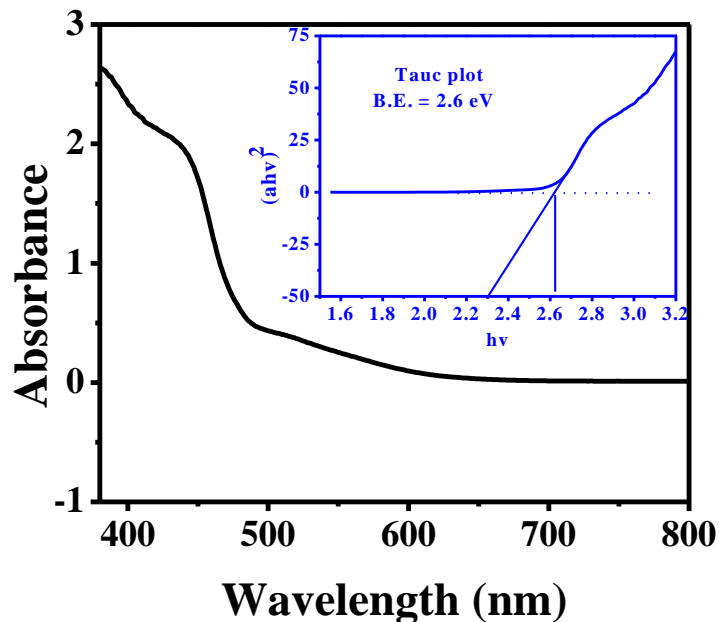


Figure 3.8: UV-visible spectrum and Tauc plot

states. The band gap value for ZnSe samples were calculated using Tauc plot which was plotted between $(\alpha h\nu)^2$ and band energy ($h\nu$).and are shown in fig. 3.8. Band gap value for ZnSe was found to be 2.6 ± 0.01 eV for all ZnSe nanostructures synthesized under various reaction conditions. Results obtained for ZnSe synthesized under different reaction conditions such as different KOH concentrations, different reaction times and finally by employing different reaction conditions are shown in figure 3.8.

3.4 Transmission electron microscopy (TEM) results

A number of TEM images were recorded by taking the samples used for XRD analysis. (as shown in figure 3.9).TEM images show that crystal facets are well defined and indicating the highly crystalline nature of NP's. TEM image shows relatively aggregates of nanoparticles of ZnSe in sample.An estimated particle size from TEM images was found to be 30 nm that was close to that measured using SEM images i.e. 28 nm.

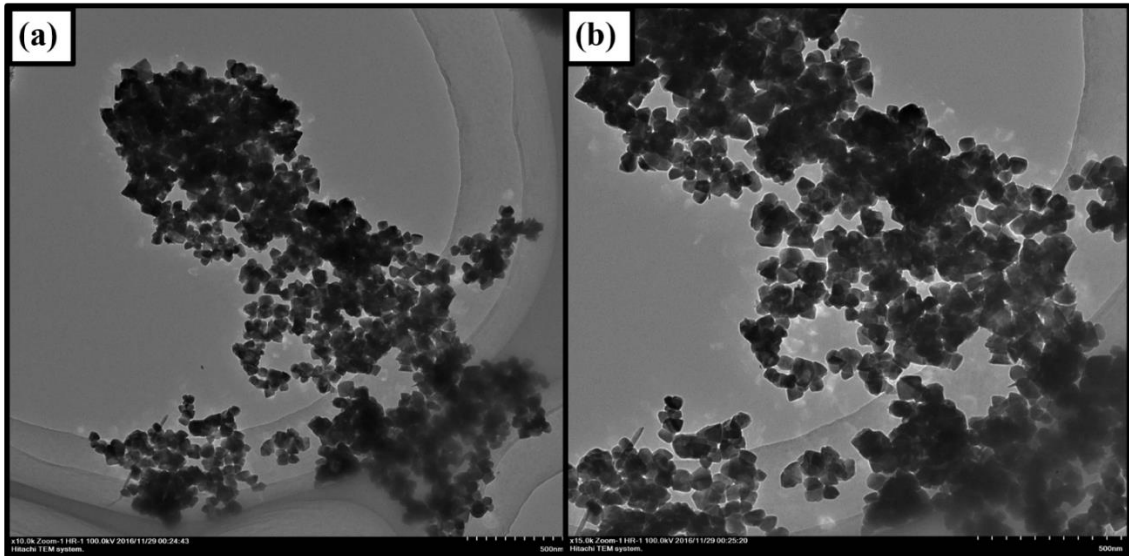


Figure 3.9 (a,b) TEM image for as synthesized ZnSe nanostructures

3.5 Compositional Analysis

Figure 3.10 shows the elemental composition of as synthesized ZnSe nanostructures. The analysis shows that sample is principally composed of ZnSe nanostructures and no additional elements are detected in sample. The ratio of Zn and Se in sample is almost 3:4. The EDS results correspond to XRD results showing that the sample is cubic blende ZnSe

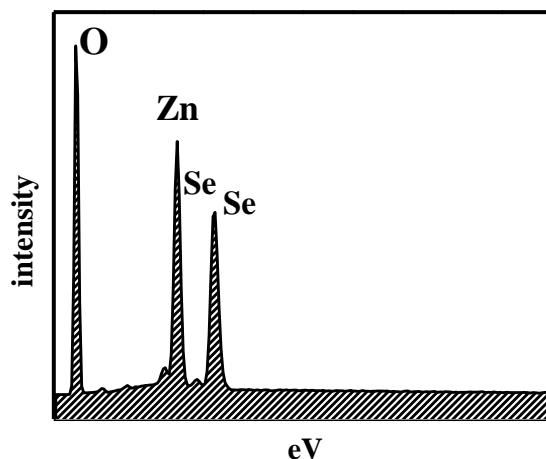


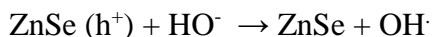
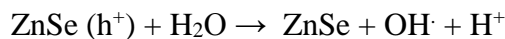
Figure 3.10: EDS spectra of ZnSe nanoparticles

3.6 Photocatalytic Activity

Photocatalysis is an emerging technology for degradation of organic dyes and pollutants. The basic principle during this process is the formation of electron and hole pairs when a photocatalyst is exposed to a light of certain wavelength which generally lies in UV and visible region. Formation of an electron/hole pair takes place when a certain semiconductor absorbs a photon of energy equal or greater than the semiconductor band gap.

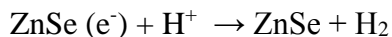
In this case the main photocatalytic activity of semiconductor rises from photoexcitation of ZnSe nanoparticles with the absorption of light energy equal or greater than band gap energy which in this case is 2.6 eV. In this case, Absorption of light greater than the band gap results in generation of electrons (e^-) in conduction band (cb) and formation of holes (h^+) take place in valence band (vb). The electrons and holes generated in the process can recombine and hence releasing the absorbed energy in form of heat. For this purpose, a sensitizer is added to semiconductor structure which can trap electron during the process. In ZnSe photocatalyst, holes can directly react with adsorbed pollutant but reaction with

water is more likely to happen due to presence of H₂O molecules in abundance in solution. In valence band, holes react with H₂O or hydroxide ions (OH⁻) to produce OH[·] radicals which is a reactive specie.



These hydroxyl ions then react with adsorbed pollutants on the surface of photocatalyst and in solution. During this process, no residue of pollutant remains and photocatalyst itself remains unaffected at the end of reaction [131].

On the other hand, e⁻ present in conduction band reacts with protons (H⁺) and reduce them to molecular hydrogen.



Photocatalytic decomposition of methanol and sodium sulfide was used as a reaction to observe the photoactivity of bare ZnSe. Photocatalytic experimental details have been mentioned earlier. In case of blank test with a photocatalyst with irradiation, no photocatalytic reaction took place. Only methanol and sodium sulphide were received at chromatograms. In case of photocatalyst without irradiation, methanol only adsorbed at catalyst surface and photoactivity was seen on GC.

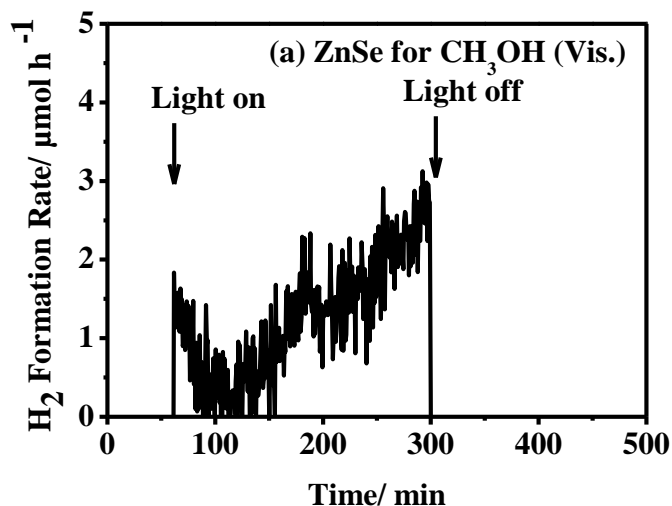


Figure 3.11 Hydrogen formation rate as a function of time of irradiation (a) when Bare ZnSe catalyst was exposed to methanol under illumination of UV light

Least rate of hydrogen rate was observed when bare ZnSe photocatalyst was exposed to methanol suspension under visible light. It was observed that the rate of hydrogen production was very low and obtained data was graph for photoactivity was unstable. This lowered rate of hydrogen formation can be attributed to rapid recombination of charge carriers i.e. electrons and holes in ZnSe photocatalyst. For this purpose, Platinum was added to ZnSe photocatalyst employing *in-situ photoreductive* conditions. Pt, in this case, acted as sink for electron capture which can reduce the rapid electron/hole recombination in photocatalyst. However, Incorporation of metal like Platinum did not change crystal structure of ZnSe. There are no diffraction peaks observed after loading of noble metal due to low loading percentage (1 % by wt.) and high dispersion on photocatalyst surface.

After the noble metal incorporation, Methanol was degraded using ZnSe/Pt photocatalyst in region of visible light. Hydrogen formation rate was found to be less than that obtained on exposure of catalyst to methanol suspension in UV-Visible range. A Maximum hydrogen generation of 6 $\mu\text{m}/\text{h}$ was seen. No significant increase or decrease was observed in H_2 formation rate on prolonged exposure to light. Low hydrogen production rate in case of visible light can be attributed to the fact that intensity of visible light is less intense than that of UV light. When metallized ZnSe (ZnSe/Pt) was exposed to methanol solution under UV/Visible light, It was observed that rate of hydrogen production increases gradually and reaches up to 30 $\mu\text{m}/\text{h}$ upon irradiation of light but prolonged

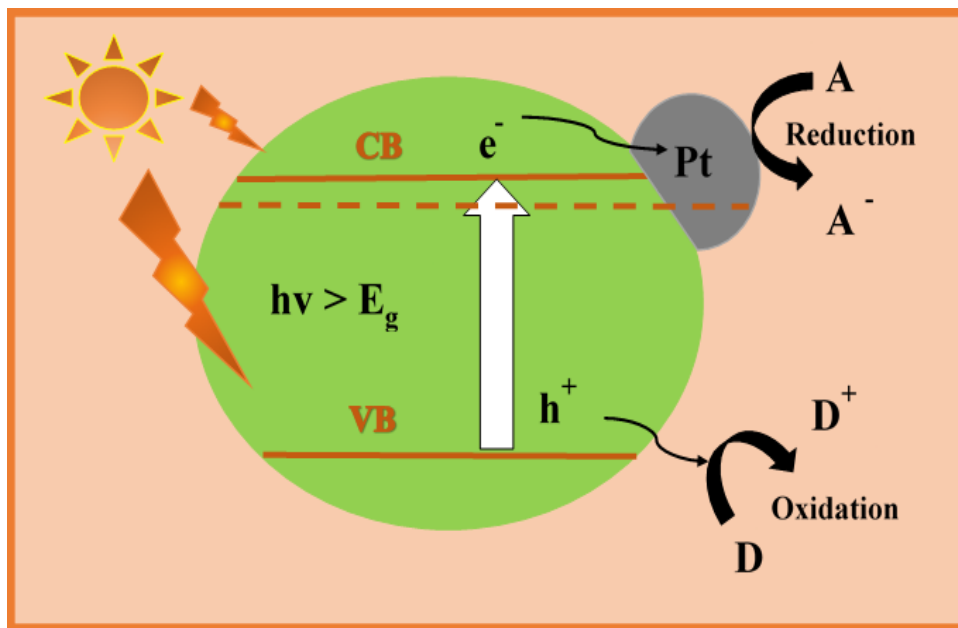


Figure 3.12 Band gap diagram of ZnSe, ZnSe/Pt photocatalyst

exposure to UV light results in slight decrease in rate of H_2 production to around 22 $\mu\text{m}/\text{h}$ after 300 min. In case of CH_3OH , photoreduction would result in formation of OH^\cdot radicals which are again very reactive and would lead to an increased photoactivity by mechanism described above. Same experiment was repeated for Sodium Sulphide suspension of Pt/ZnSe. When Sodium Sulphide was exposed to UV and visible light, a maximum hydrogen production rate upto 17 $\mu\text{m}/\text{h}$ was observed which decreased slightly after an irradiation time of 300 minutes. Less activity in Na_2S when compared with

CH₃OH could be due to absence of any OH⁻ group in its structure which is a very reactive specie in degradation of a pollutant. In all cases with ZnSe/Pt as photocatalyst, Photoactivity was found to be better than bare ZnSe which can attributed to the presence of Pt noble metal in photocatalyst structure.

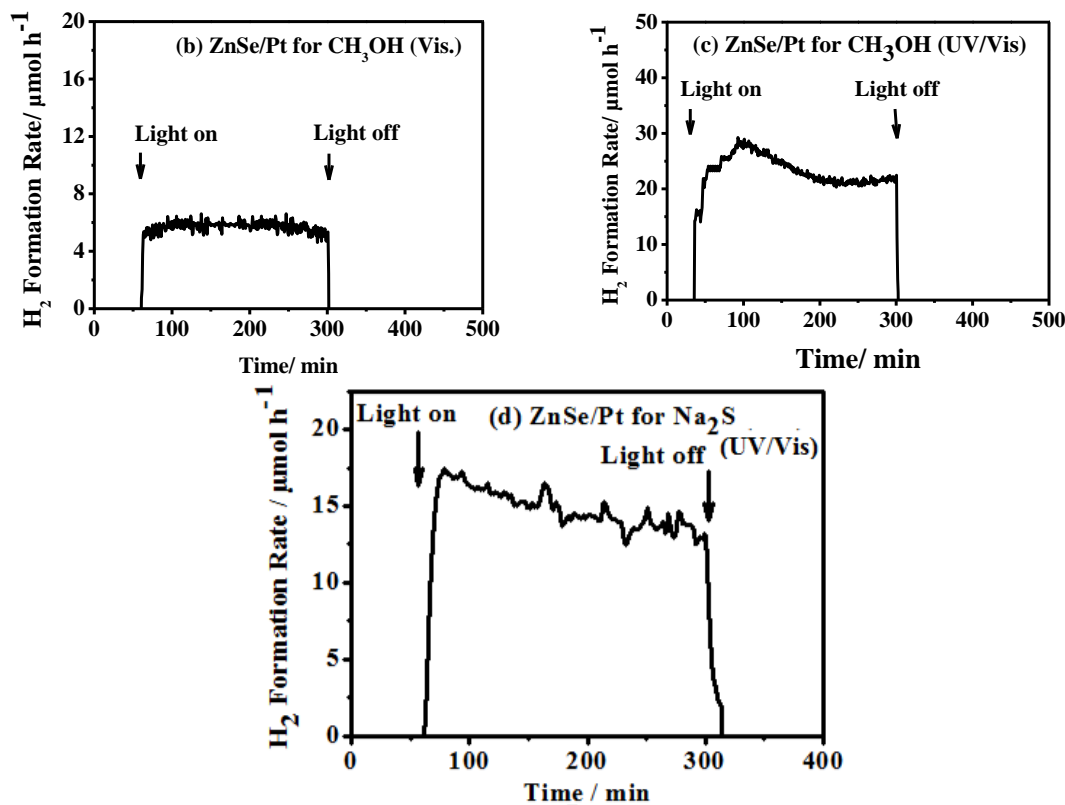


Figure 3.13 (b) Pt/ZnSe exposed to methanol solution under illumination of visible sunlight (c) when Pt/ZnSe exposed to Methanol solution under illumination of UV/Visible light (d) ZnSe/Pt exposed to sodium sulphide solution under illumination of UV and visible light.

In all reactions given above, it took about 30 to 40 minutes to reach at a stage of maximum hydrogen formation rate.

Chapter 4

Conclusions and Future Prospects

4.1 Conclusions and Future Prospects

In this study, it was found that hydrothermal route can be used to successfully synthesize ZnSe nanostructured based semiconductor photocatalyst. The composition, morphology, geometry, crystal structure and crystallite size of materials have been investigated by employing XRD, EDX spectra, SEM and the TEM analysis. Optical properties of sample was studied using UV-Vis spectroscopy. XRD studies revealed cubic structure of ZnSe nanoparticles while SEM and TEM studies showed spherical shape of particles. Optical properties show that a semiconductor photocatalyst with band gap of 2.6 eV has been synthesized. The same photocatalyst was synthesized by changing different reaction conditions like reaction temperature, reaction time and KOH concentration to study the effect of these parameters on particle size and morphology. It was seen that reaction time has less effect on particle size of synthesized sample when compared with samples synthesized by changing reaction time and reducing agent concentration.

Afterwards, the synthesized photocatalyst was used for production of Hydrogen and simultaneously degradation of two dyes that were Sodium Sulphide and Methanol and was found successful. ZnSe photocatalyst was doped with Platinum metal to reduce the rapid e/h recombination and to increase the efficiency in term of hydrogen production and dye degradation, which was found to be a successful strategy as rate of hydrogen production increased from 3 μ m/h to 30 μ m/h. The Photocatalytic activity was firstly checked for UV region and then for whole UV-Visible range.

In future, the synthesized semiconductor photocatalyst can be used for reduction of Carbon dioxide. ZnSe photocatalyst can also be combined with other noble metal like Ag and Au in future to examine the results of hydrogen production and dye degradation.

REFERENCES

- [1] Moniz S. ,Shevlin S.A. ,Martin, D. ,Guo Z.,Tang J. ,“Visible-Light Driven Heterojunction Photocatalysts for Water Splitting—A Critical Review”. *Energy Environ. Sci.*,vol. 8,p 731–759,2015.
- [2] Byrne J., Hughes K., Rickerson W., Kurdgelashvili L, “American policy conflict in the green house: Divergent trends in federal, regional, state, and local green energy and climate change policy”. *Energy Policy*,Vol. 35,p 4555–4573,2007.
- [3] Solomon S., Plattner G.-K.G., Knutti R., Friedlingstein P., “Irreversible climate change due to carbon dioxide emissions.” *Proc. Natl. Acad. Sci. USA* ,Vol. 106,p 1704– 1709,2009.
- [4] Di Primio, R. Horsfield, B. Guzman-Vega, “Determining the temperature of petroleum formation from the kinetic properties of petroleum asphaltenes”, *Nature*, Vol. 406,p. 173– 176,2000.
- [5] Dincer I., Zamfirescu C., Dinçer I., Zamfirescu C., Dincer I., Zamfirescu C., “Sustainable Energy Systems and Applications”, *Springer Science & Business Media: New York, NY, USA*, Volume 6,2011.
- [6] Parida B., Iniyar S., Goic R., “A review of solar photovoltaic technologies.”, *Renew. Sustain. Energy Rev.*,Vol. 15, 1625–1636,2011.
- [7] Xie W.T., Dai Y.J., Wang R.Z., Sumathy K., “Concentrated solar energy applications using Fresnel lenses: A review”, *Renew. Sustain. Energy Rev.* ,Vol. 15, 2588–2606,2011.
- [8] Zamfirescu Dincer I., Naterer G.F., Banica R., “Quantum efficiency modeling and system scaling-up analysis of water splitting with $Cd_{1-x}Zn_xS$ solid-solution photocatalyst”, *Chem. Eng. Sci.*,Vol. 97,p 235–255,2013.
- [9] Chong M.N., B. Jin, C.W.K. Chow and C. Saint, *Water Res.*, Vol. 44, 2997, 2010.

- [10] Fujishima A., Honda K., “Electrochemical photolysis of water at a semiconductor electrode”, *Nature*, Vol. 238,p 37–38,1972.
- [11] Turner J., “A Sustainable hydrogen production.” , *Science*,Vol. 305,p 972–974,2004.
- [12] Hou K., Hughes R., “The kinetics of methane steam reforming over a Ni/ α -Al₂O₃ catalyst”, *Chem. Eng. J.* ,Vol. 82,p 311–328,2001.
- [13] Czernik S., Evans R., French R., “Hydrogen from biomass-production by steam reforming of biomass pyrolysis oil”, *Catal. Today* ,Vol. 129,p 265–268,2007.
- [14] Xie Q., Wang Y., Pan B., Wang H., Su W., Wang X., “A novel photocatalyst LaOF: Facile fabrication and photocatalytic hydrogen production”, *Catal. Commun.*, Vol. 27,p 21– 25,2012.
- [15] Luo J., Im J.-H., Mayer M.T., Schreier M., Nazeeruddin M.K., Park N.-G., Tilley S.D., Fan H.J., Gratzel, M., “Water photolysis at 12.3% efficiency via perovskite photovoltaics and Earth-abundant catalysts”, *Science*, Vol. 345,p 1593–1596,2014.
- [16] Wu N.L., Lee M.S., “Enhanced TiO₂ photocatalysis by Cu in hydrogen production from aqueous methanol solution”, *Int. J. Hydrog. Energy*, Vol. 29,p 1601–1605,2004.
- [17] Steinfeld A., “Solar hydrogen production via a two-step water-splitting thermochemical cycle based on Zn/ZnO redox reactions”, *Int. J. Hydrog. Energy* ,Vol. 27,p 611–619,2002.
- [18] Akkerman I., Janssen M., Rocha J., Wijffels R.H., “Photobiological hydrogen production: Photochemical efficiency and bioreactor design”, *Int. J. Hydrog. Energy*, Vol. 27,p 1195–1208,2002.
- [19] Das D., Veziroglu T.N., “Advances in biological hydrogen production processes”, *Int. J. Hydrog. Energy* ,Vol. 33,p 6046–6057,2008.

- [20] Guan Y., Deng M., Yu X., Zhang W., “Two-stage photo-biological production of hydrogen by marine green alga *Platymonas subcordiformis*”, *Biochem. Eng. J.*, Vol. 19, p 69–73, 2004.
- [21] Lewis N.S., Nocera D.G., “Powering the planet: Chemical challenges in solar energy utilization”, *Proc. Natl. Acad. Sci. USA*, Vol. 103, p 15729–15735, 2006.
- [22] Kudo A., “Photocatalysis and solar hydrogen production”, *Pure Appl. Chem*, Vol. 79, p 1917–1927, 2007.
- [23] Paramasivan Gomathisankar, Tomoko Noda, Hideyuki Katsumata, Tohru Suzuki, Satoshi Kaneco, “Enhanced hydrogen production from aqueous methanol solution using TiO₂/Cu as photocatalysts”, *Front. Chem. Sci. Eng.*, Vol. 8(2): 197–202, 2014.
- [24] A. Perez-Larios, R. Lopez, A. Hernandez-Gordillo, F. Tzompantzi, R. Gomez, L.M. Torres-Guerra, “Improved hydrogen production from water splitting using TiO₂–ZnO mixed oxides photocatalysts”, *Fuel*, Vol. 100, p. 139–143, 2012.
- [25] Z. Khan, M. Qureshi, “Tantalum doped BaZrO₃ for efficient photocatalytic hydrogen generation by water splitting”, *Catalysis Communications*, Vol. 28, p. 82–85, 2012.
- [26] L.M. Torres-Martínez, R. Gómez, O. Vázquez-Cuchillo, I. Juárez-Ramírez, A. CruzLópez, F.J. Alejandro-Sandoval, “Enhanced photocatalytic water splitting hydrogen production on RuO₂/La:NaTaO₃ prepared by sol–gel method”, *Catalysis Communications*, Vol. 12, p. 268–272, 2010.
- [27] Yang Liua., Lei Xiea, Yan Li, Rong Yanga, Jianglan Qua, Yaoqi Li, Xingguo Li, “Synthesis and high photocatalytic hydrogen production of SrTiO₃ nanoparticles from water splitting under UV irradiation”, *Journal of Power Sources*, Vol. 183, p. 701–707, 2008.
- [28] Chanjuan Xing, Yaojun Zhang, Wei Yan, Liejin Guo, “Band structure-controlled solid solution of Cd_{1-x} Zn_xS photocatalyst for hydrogen production by water splitting”, *International Journal of Hydrogen Energy*, Vol. 31, p. 2018 – 2024, 2006.

- [29] Shukla SP, Gupta GS , “Toxic effects of omega chrome red ME and its treatment by adsorption”, *Ecotoxicol Environ Saf* , Vol. 24,p.155–163,1992. [35] Slokar YM, Marechal AML , “Methods of decoloration of textile wastewaters” Vol. 37,p 335–356,1998.
- [30] Legrini O, Oliveros E, Braun AM , “Photochemical processes for water treatment”, *Chem Rev* ,Vol. 93,p 671–698,1993.
- [31] Hassan ME, Chen J, Liu G, Zhu D, Cai J, “Enhanced photocatalytic degradation of methyl orange dye under the daylight irradiation over CN-TiO₂ modified with OMS-2”, *Materials*, Vol. 7, p. 8024–8036,2014.
- [32] Al-Harbi LM, Kosa SA, Abd El Maksod IH, Hegazy EZ, “The photocatalytic activity of TiO₂-Zeolite composite for degradation of dye using synthetic UV and Jeddah sunlight”, *J Nanomater* ,Vol. 15,p. 1–6,2015.
- [33] Kim S, Hwang SJ, Choi W, “Visible Light Active Platinum-Ion Doped TiO₂ Photocatalyst”, *J Phys Chem B* ,Vol. 109, p. 24260–24267,2005.
- [34] Nicoleta Liliana Olteanu, Elena Adina Rogozea, Simona Andreea Popescu, Adina Roxana Petcu, Cosmina Andreea Laz̃ar, Aurelia Meghea, Maria Mihaly, “One-step synthesis of Au-ZnO-SiO₂ nanostructures”, *Journal of Molecular Catalysis A: Chemical*,2016.
- [35] Khizar Hayat, M.A. Gondal, Mazen M. Khaleda, Shakeel Ahmed, Ahsan M. Shemsid, “Nano ZnO synthesis by modified sol gel method and its application in heterogeneous photocatalytic removal of phenol from water”, *Applied Catalysis A: General*,Vol. 393,p 122–129,2011.
- [36] Weifeng Yao , Jinhua Ye, “Photocatalytic properties of CaBiVMO₈ compounds”, *Catalysis Today*,Vol. 116,p 18–21,2006.
- [37] Hai-Xia Wang , Rong Wua., Shun-Hang Wei , Li-Rui Yu , Ji-Kang Jian , Juan Hou , Jing Wang, Hong-Yan Zhang, Yan-Fei Sun, “One-pot solvothermal synthesis of

- ZnTe/RGO nanocomposites and enhanced visible-light photocatalysis”, *Chinese Chemical Letters*, 2016.
- [38] Jiade Lia, Wen Fang, Changlin Yua,, Wanqin Zhoua,, Lihua zhua, Yu Xied, “Ag-based semiconductor photocatalysts in environmental purification”, *Applied Surface Science*, Vol. 358, p 46–56, 2015.
- [39] W.G. Wang, B. Cheng, J.G. Yu, G. Liu, W.H. Fan, *Asian J. Chem.*, Vol. 7, p 1902–1908, 2012.
- [40] Ke-Jian Ju, Ming Zhang, Qian-Li Zhang, JieWei, Ai-Jun Wang, “Facile Synthesis of Rambutan-Like ZnO Hierarchical Hollow Microspheres with Highly Photocatalytic Activity”, *Journal of Nanomaterials*, 2015.
- [41] Alireza Nezamzadeh-Ejehieha, Maryam Karimi-Shamsabadi, “Comparison of photocatalytic efficiency of supported CuO onto micro and nano particles of zeolite X in photodecolorization of Methyleneblue and Methyl orange aqueous mixture”, *Applied Catalysis A: General*, Vol. 477, p 83–92, 2014.
- [42] Thi Hiep Nguyen, Thu Loan Nguyen, Thi Dieu Thuy Ung, Quang Liem Nguyen, “Synthesis and characterization of nano-CuO and CuO/TiO₂ photocatalysts”, *Adv. Nat. Sci.: Nanosci. Nanotechnol.*, Vol. 4, 2013.
- [43] Ayman Yousef, Nasser A.M. Barakat, Touseef Amnaa, Afeesh R. Unnithan, Salem S. Al-Deyab, Hak Yong Kim, “Influence of CdO-doping on the photoluminescence properties of ZnO nanofibers: Effective visible light photocatalyst for waste water treatment”, *Journal of Luminescence*, Vol. 132, p 1668–1677, 2012.
- [44] Bing Cao, Guisheng Li, Hexing Li, “Hollow spherical RuO₂/TiO₂/Pt bifunctional photocatalyst for coupled H₂ production and pollutant degradation”, *Applied Catalysis B: Environmental*, Vol. 194, p. 42–49, 2016.
- [45] Rajendran Kalyani Karuppasamy Gurunathan, “PTh-rGO-TiO₂ Nanocomposite for Photocatalytic Hydrogen Production and Dye Degradation”, *Journal of Photochemistry and Photobiology A: Chemistry*, 2016.

- [46] Hong Gao, Junying Zhanga, Rongming Wang, Mei Wang, “Highly efficient hydrogen production and formaldehyde degradation by Cu₂O microcrystals”, *Applied Catalysis B: Environmental*, Vol. 172–173, p. 1–6, 2015.
- [47] Xi Wang, Wen-chao Peng, Xiao-yan Li, “Photocatalytic hydrogen generation with simultaneous organic degradation by composite CdSeZnS nanoparticles under visible light”, *International journal of hydrogen energy*, Vol. 39, p. 13454-13461, 2014.
- [48] Yasser A. Shaban, “Simultaneous Hydrogen Production with the Degradation of Naphthalene in Seawater Using Solar Light-Responsive Carbon-Modified (CM)-n-TiO₂ Photocatalyst”, *Modern Research in Catalysis*, Vol. 2, p. 6-12, 2013.
- [49] Alexia Patsoura, Dimitris I. Kondarides, Xenophon E. Verykios, “Photocatalytic degradation of organic pollutants with simultaneous production of hydrogen”, *Catalysis Today*, Vol. 124, p. 94–102, 2007.
- [50] H. Tong, S. X. Ouyang, Y. P. Bi, N. Umezawa, M. Oshikiri and J. H. Ye, *Adv. Mater.*, Vol. 24, p 229, 2012.
- [51] Murdoch M., Waterhouse G. I. N., Nadeem M. A., Metson J. B., Keane M. A., Howe R. F., Llorca J., Idriss H., *Nat. Chem*, Vol. 3, p 489, 2011.
- [52] Carp O., Huisman C. L., Reller A., *Prog. Solid State Chem.*, Vol. 32, 2004.
- [53] Ma B.J., Wen F.Y., Jiang H.F., Yang J.H., Ying P.L., Li C., “The Synergistic Effects of Two Co-Catalysts on Zn₂GeO₄ on Photocatalytic Water Splitting.”, *Catal. Lett.*, Vol. 134, p 78–86, 2010.
- [54] Wang D., Li R., Zhu J., Shi J., Han J., Zong X., Li C., “Photocatalytic Water Oxidation on BiVO₄ with the Electro catalyst as an Oxidation Cocatalyst: Essential Relations between Electrocatalyst and Photocatalyst.”, *J. Phys. Chem. C*, Vol. 116, p 5082–5089, 2012.
- [55] Maeda K., Xiong A. K., Yoshinaga T., Ikeda T., Sakamoto N., Hisatomi T., Takashima M., Lu D.L., Kanehara M., Setoyama T., Teranishi T., Domen K., “Photocatalytic Overall Water Splitting Promoted by Two Different Cocatalysts for

Hydrogen and Oxygen Evolution under Visible Light”, *Angew. Chem., Int. Ed.*, Vol. 49, p 4096–4099, 2010.

[56] Kwon BH, Jang HS, Yoo HS, Kim SW, Kang DS, Maeng S, Jang DS, Kim H, Jeon DY, “White-light emitting surface-functionalized ZnSe quantum dots: europium complex-capped hybrid nanocrystal”, *J. Mater. Chem.*, Vol. 21, p 12812-12818, 2011.

[57] Sharma VK, Guzelurk B, Erdem T, Kelestemur Y, Demir HV, “Tunable White-Light-Emitting Mn-Doped ZnSe Nanocrystals”, *ACS Appl. Mater. Interfaces*, Vol. 6, p. 3654–3660, 2014.

[58] Shao PT, Wang HZ, Zhang QH, Li YG, “White light emission from Mn-doped ZnSe d-dots synthesized continuously in microfluidic reactors”, *J. Mater. Chem* Vol. 21, p. 17972-17977, 2011.

[59] Chen GH, Ho SJ, Chen HS, “Cubic Zinc blende ZnSe Nanowires with an Entangling Structure Grown via Oriented Attachment and Their Application in Organic–Inorganic Heterojunction Light-Emitting Diodes” ,*J. Phys. Chem C* ,Vol. 118, p. 25816-25822, 2014.

[60] Wood V, Halpert JE, Panzer MJ, Bawendi MG, Bulovic V, “Alternating current driven electroluminescence from ZnSe/ZnS:Mn/ZnS nanocrystals”, *Nano Lett*, Vol. 9, p. 2367-2371, 2009.

[61] Ji WY, Jing PT, Xu W, Yuan X, Wang YJ, Zhao JL, Jen AKY, “High color purity ZnSe/ZnS core/shell quantum dot based blue light emitting diodes with an inverted device structure”, *Appl. Phys. Lett*, Vol. 103, 2013.

[62] Justice J, Bower C, Meitl M, Mooney MB, Gubbins MA, Corbett B, “Wafer-scale integration of group III–V lasers on silicon using transfer printing of epitaxial layers”, *Nat. Photonics*, Vol. 6, p. 610-614, 2012.

[63] Liu X, Zhang Q, Xiong Q, Sum TC, “Tailoring the lasing modes in semiconductor nanowire cavities using intrinsic self-absorption”, *Nano Lett*, Vol. 13, p. 1080-1085, 2013.

- [64] Feng GY, Yang C, Zhou SH, “Nanocrystalline Cr²⁺-doped ZnSe Nanowires Laser”, *Nano Lett*, Vol. 13, p. 272–275, 2013.
- [65] Duan XF, Huang Y, Agarwa R, Lieber CM, “Single-nanowire electrically driven lasers”, *Nature*, Vol. 421, p. 241-245, 2003.
- [66] Chu S, Wang GP, Zhou WH, Lin YQ, Chernyak L, Zhao JZ, Kong JY, Li L, Ren JJ, Liu JL, “Electrically pumped waveguide lasing from ZnO nanowires”, *Nat. Nanotechnol*, Vol. 6, p. 506-510, 2011.
- [67] Zhai TY, Li L, Wang X, Fang XS, Bando Y, Golberg D., “Recent Developments in One-Dimensional Inorganic Nanostructures for Photodetectors”, *Adv. Mater*, Vol. 20, p. 4233-4248, 2010.
- [68] Zhai TY, Fang XS, Liao MY, Xu XJ, Zeng HB, Bando Y, Golberg D., “A Comprehensive Review of One-Dimensional Metal-Oxide Nanostructure Photodetectors”, *Sensors*, Vol. 9, p. 6504-6529, 2009.
- [69] Soci C, Zhang A, Bao XY, Kim H, Lo Y, Wang D., “Nanowire Photodetectors”, *J. Nanosci. Nanotechnol*, Vol. 10, p. 1430-1439, 2010.
- [70] Zhai TY, Fang XS, Bando Y, Dierre B, Liu BD, Zeng HB, Xu XJ, Huang Y, Yuan XL, Sekiguchi T, Golberg D., “Characterization, cathodoluminescence, and field-emission properties of morphology-tunable CdS micro/nanostructures”, *Adv. Funct. Mater*, Vol. 19, p. 2423-2430, 2009.
- [71] Zhai TY, Li L, Ma Y, Liao MY, Wang X, Fang XS, Yao JN, Bando Y, Golberg D., “One-dimensional inorganic nanostructures: synthesis, field-emission and photodetection”, *Chem. Soc. Rev*, Vol. 40, p. 2986-3004, 2011.
- [72] Fang XS, Bando Y, Gautam UK, Ye CH, Golberg D., “Inorganic semiconductor nanostructures and their field-emission applications”, *J. Mater. Chem*, Vol. 18, p. 5095-5102, 2008.

- [73] Zhao LJ, Pang Q, Cai Y, Wang N, Ge WK, Wang JN, Yang SH, “Vertically aligned zinc selenide nanoribbon arrays: microstructure and field emission”, *J. Phys. D: Appl. Phys*, Vol. 40, p. 3587–3591,2007.
- [74] Leung YP, Choy WCH, Yuk TI, “Linearly resistive humidity sensor based on quasi one-dimensional ZnSe nanostructures”, *Chem. Phys. Lett*, Vol. 457, p. 198-201,2008.
- [75] Yan W, Hu CG, Xi Y, Wan BY, He XS, Zhang MC, Zhang Y., “ZnSe nanorods prepared in hydroxide-melts and their application as a humidity sensor”, *Mater. Res. Bull*, Vol. 44, p. 1205-1208,2009.
- [76] Strelcov E, Lilach Y, Kolmakov A., “Gas Sensor Based on Metal-Insulator Transition in VO₂ Nanowire Thermistor”, *Nano Lett*, Vol. 9, p. 2322–2326,2009.
- [77] Park S, Kim S, Lee WI, Kim KK, Lee C., “Room temperature, ppb-level NO₂ gas sensing of Multiple networked ZnSe nanowire sensors under UV illumination”, *Beilstein J. Nanotechnol*, Vol. 5, p.1836–1841,2014.
- [78] Ip KM, Liu Z, Ng CM, Hark SK., “Effects of passivation and ambient gases on the photoluminescence of ZnSe nanowires”, *Nanotechnol*, Vol. 16, p. 1144-1147,2006.
- [79] Wang X, Liao M, Zhong YT, Zheng JY, Tian W, Zhai TY, Zhi CY, Ma Y, Yao JN, Bando Y, Golberg D., “ZnO Hollow Spheres with Double-Yolk Egg Structure for HighPerformance Photocatalysts and Photodetectors”, *Adv. Mater*, Vol. 24,p. 3421–3425,2012.
- [80] Yao TT, Zhao Q, Qiao ZP, Peng F, Wang HJ, Yu H, Chi C, Yang J., “Chemical Synthesis, Structural Characterization, Optical Properties, and Photocatalytic Activity of Ultrathin ZnSe Nanorods”, *Chem. Eur. J*, Vol. 17, p. 8663-8670,2011.
- [81] Xiong SL, Xi BJ, Wang CM, Xi GC, Liu XY, Qian YT., “Solution-Phase Synthesis and High Photocatalytic Activity of Wurtzite ZnSe Ultrathin Nanobelts: A

General Route to 1D Semiconductor Nanostructured Materials”, *Chem. Eur. J.*, Vol. 13, p. 7926-7932,2007.

[82] Li L, Zhai TY, Bando Y, Golberg D., “Recent progress of one-dimensional ZnO nanostructured solar cells”, *Nano Energy*, Vol, 1, p. 91-106,2012.

[83] Yu R, Lin QF, Leung SF, Fan ZY., “Nanomaterials and nanostructures for efficient light absorption and photovoltaics”, *Nano Energy*, Vol. 1, p. 57-72,2012.

[84] Fan ZY, Razavi H, Do JW, Moriwaki A, Ergen O, Chueh YL, Leu PW, Ho JC, Takahashi T, Reichertz LA, Neale S, Yu K, Wu M, Ager JW, Javey A., “Threedimensional nanopillar-array photovoltaics on low-cost and flexible substrates”, *Nat. Mater*, Vol. 8, p. 648-653,2009.

[85] Tang JY, Huo ZY, Brittman S, Gao HW, Yang PD., “Solution-processed core-shell nanowires for efficient photovoltaic cells”, *Nat. Nanotechnol*, Vol. 6, p. 568-572,2011.

[86] Liu, XL, Liang S, Nan F, Yang ZJ, Yu XF, Zhou L, Hao ZH, Wang QQ., “Solutiondispersible Au nanocube dimers with greatly enhanced two-photon luminescence and SERS” ,*Nanoscale*, Vol. 5, p. 5368-5374,2013.

[87] Brunetti V, Chibli H, Fiammengo R, Galeone A, Malvindi MA, Vecchio G, Cingolani R, Nadeau JL, Pompa PP., “InP/ZnS as a safer alternative to CdSe/ZnS core/shell quantum dots: in vitro and in vivo toxicity assessment”, *Nanoscale*, Vol. 5, p. 307317,2013.

[88] Wang C, Gao X, Su XG., “In vitro and in vivo imaging with quantum dots”, *Anal. Bio ana. Chem*, Vol. 397, p. 1397-1415,2010.

[89] Gao XH, Yang LL, Petros JA, Marshall FF, Simons JW, Nie SM., “In vivo molecular and cellular imaging with quantum dots”, *Curr. Opin. Biotech*, Vol. 16, p. 63-72,2005.

- [90] Regulacio MD, Han MY., “Composition-Tunable Alloyed Semiconductor Nanocrystals”, *Accounts of Chemical Research*, Vol. 43, p. 621-630,2010.
- [91] Charvet N, Reiss P, Roget A, Dupuis A, Grunwald D, Carayon S, Chandezona F, Livache T., “Biotinylated CdSe/ZnSe nanocrystals for specific fluorescent labeling”, *J. Mater. Chem*, Vol. 14, p. 2638-2642,2004.
- [92] Saikia K, Deba P, Kalita E., “Sensitive fluorescence response of ZnSe(S) quantum dots: an efficient fluorescence probe”, *Phys. Scr*, Vol. 87, p. 065802,2013.
- [93] Klaus T., Joerger R., Olsson E. and Granqvist C.G., “SilverBased Crystalline Nanoparticles, Microbially Fabricated”, *J. Proc. Natl. Acad. Sci. USA*,Vol. 96,p. 1361113614,1999.
- [94] Konishi Y. and Uruga T., “Bioreductive Deposition of Platinum Nanoparticles on the Bacterium *Shewanella algae*”, *J. Biotechnol.*,Vol. 128,p. 648-653,2007.
- [95] Willner I, Baron R. and Willner B., “Growing metal nanoparticles by enzymes”, *J. Adv. Mater*,Vol. 18,p. 1109-1120,2006.
- [96] Vigneshwaran N., Ashtaputre N.M., Varadarajan P.V, Nachane R.P., Paralikar K.M., Balasubramanya R.H., *Materials Letters*,Vol. 61,p. 1413-1418,2007.
- [97] Shankar S.S., Ahmed A., Akkamwar B., Sastry M., Rai A., Singh A., “Biological synthesis of triangular gold nanoprism”, *Nature*,Vol. 3,p. 482,2004.
- [98] Ahmad N., Sharma S., Singh V.N., Shamsi S.F, Fatma A. and Mehta B.R., “Biosynthesis of silver nanoparticles from *Desmodium triflorum* : a novel approach towards weed utilization”, *Biotechnol. Res. Int* ,454090 (1-8),2011.
- [99] Tissue, B.M. and Yuan H.B. , “ Structure particle size and annealing gas phasecondensed $\text{Eu}^{3+} : \text{Y}_2\text{O}_3$ nanophosphors ”, *J. Solid State Chemistry*, Vol. 171, pp 12- 18,2003.

- [100] Hasany, S.F., Ahmad, I., Ranjan, J. & Rehman, A., "Systematic review of the preparation techniques of Iron oxide Magnetic Nanoparticles", *Nanoscience & Nanotechnology*, Vol. 2(6), pp 148-158.,2012.
- [101]. Gohil, S., Chandra, R., Chalke, B., Bose, S. & Ayyub, P., "Sputter deposition of self-organised nanoclusters through porous anodic alumina templates", *J. Nanoscience Nanotech.*, Vol. 7, pp 641646,2007.
- [102] Chang, W., Skandan, G., Hahn, H., Danforth, S.C. and Kear, B.H., "Chemical vapor condensation of nanostructured ceramic powders", *Nanostructured Materials*, vol. 4(3), pp345- 351,1994.
- [103] Winterer, M. and Hahn, H., *Metallkd, Z.*, " Chemical Vapor Synthesis of Nanocrystalline Powders ", *Nanoceramics by Chemical Vapor Synthesis*, vol. 94, pp1084-1090,2003.
- [104] Konrad ,A., Herr, U., Tidecks, R. and Samwer, F., " Luminescence of bulk and nanocrystalline cubic yttria", *J. of Appl. Phys.*, vol. 90(7) , pp3516-3523,2001.
- [105] Rostislav, A. Andrievskii," The synthesis and properties of nanocrystalline refractory compounds" *Russ. Chem. Rev.*, vol.63, pp411-427,1994.
- [106] Sharma, A.B., Sharma, M. and Pandey,R.K.," Synthesis, Properties and Potential Applications of Semiconductor Quantum Particles" , *Asian Journal of Chemistry*, vol.21(10) , pp 033-038,2009.
- [107] Bhargava, R.N., Gallagher, D., Hong, X. and Nurmikko, A.," Optical properties of manganese-doped nanocrystals of ZnS", *Physical Review Letters*, vol.72, pp416419,1994.

- [108] Yu, Z.Q., Chang, D., Li, C., Zhang, N., Feng, Y.Y. and Dai, Y.Y., "Blue photoluminescent properties of pure nanostructured γ -Al₂O₃" *Material Research Society*, vol.16(7), pp1890-1893, 2001
- [109] Lu, C.H. and Jagannathan, J., "Cerium-ion-doped yttrium aluminum garnet nanophosphors prepared through sol-gel pyrolysis for luminescent lighting," *Applied Physics Letters*, vol.80(19), pp3608-3610, 2002.
- [110] Morita, M., Rau, D., Kajiyama, S., Sakurai, T., Baba, M. and Iwamura, M., "Luminescence properties of nano-phosphors: metal-ion doped sol-gel silica glasses" *Materials Science-Poland*, vol.22(1), pp 515, 2004.
- [111] Cullity BD, Stock SR, *Elements of X-ray Diffraction*, 3rd Edition, New York: Prentice Hall, 2001.
- [112] S.L. Xue, S.X. Wu, Q.Z. Zeng., Synthesis, field emission properties and optical properties of ZnSe nanoflowers, *Applied Surface Science*, 2016.
- [113] N.A. Ab Aziza, P. Palaniandy, H.A. Aziza, I. Dahlanb, Review of the mechanism and operational factors influencing the degradation process of contaminants in heterogeneous photocatalysis, *Journal of Chemical Research*, Vol. 40, 704–712, 2016.